

Peccei-Quinn NMSSM in the light of 125 GeV Higgs

Kyu Jung Bae^{a,*}, Kiwoon Choi^{a,b,†}, Eung Jin Chun^{b,‡}, Sang Hui Im^{a,§},
Chan Beom Park^{c,¶}, and Chang Sub Shin^{d,||}

^a*Department of Physics, KAIST, Daejeon 305-701, Korea*

^b*Korea Institute for Advanced Study, Seoul 130-722, Korea*

^c*Instituto de Física Teórica UAM/CSIC,
Universidad Autónoma de Madrid, Cantoblanco, 28049 Madrid, Spain*

^d*Asia Pacific Center for Theoretical Physics,
Pohang, Gyeongbuk 790-784, Republic of Korea*

ABSTRACT

We study the phenomenology of the Peccei-Quinn invariant extension of the next-to-minimal supersymmetric standard model (NMSSM) in view of the recent discovery of a 125 GeV Higgs boson. The minimal model having no quadratic and cubic terms of the NMSSM singlet field predicts a light singlino-like lightest supersymmetric particle (LSP). The model is strongly disfavored considering the Higgs invisible decay and the dark matter characteristic of the LSP in the standard cosmology. However, the saxion, a CP-even companion of the axion in the Peccei-Quinn sector, can cause a late-time entropy production to suppress the dangerous thermal LSP density eliminating the problems with the LSP dark matter. The collider signal of the model contains multi-jet and $h/W/Z$ plus missing energy, which can be discovered in the early stage of the 14 TeV LHC running.

*Email: kyujung.bae@kaist.ac.kr

†Email: kchoi@kaist.ac.kr

‡Email: ejchun@kias.re.kr

§Email: shim@muon.kaist.ac.kr

¶Email: chanbeom.park@csic.es

||Email: csshin@apctp.org

1 Introduction

The strong CP problem can be nicely resolved in a supersymmetric (SUSY) standard model, which allows an extended Higgs sector to implement the Peccei-Quinn (PQ) symmetry [1]. After integrating out the heavy PQ sector around $v_{\text{PQ}} = 10^9 - 10^{12}$ GeV, the low energy theory can be reduced to the conventional minimal supersymmetric standard model (MSSM) [2], or to the next-to-minimal supersymmetric standard model (NMSSM) [3] as proposed recently in [4, 5].

In the PQ-symmetric NMSSM (PQ-NMSSM), the low-energy theory is generically described by the superpotential,

$$W = \lambda S H_u H_d + \mu_S^2 S + \frac{1}{2} \mu'_S S^2, \quad (1)$$

and corresponding soft-breaking terms in the scalar potential, where μ_S and μ'_S at the TeV scale can arise as a function of v_{PQ} after the PQ symmetry breaking at the scale v_{PQ} .

In this paper, we investigate the phenomenology of the PQ-NMSSM in light of the recent LHC results on the Higgs boson search [6, 7]. In its minimal form [4], the model contains only the μ_S^2 term predicting a very light singlino. Because of this, the minimal model is severely constrained by the consideration of the Higgs invisible decay and the dark matter property of the singlino-like lightest supersymmetric particle (LSP) in the standard cosmology. A sizable NMSSM contribution to the 125 GeV Higgs boson mass can be obtained with $\tan \beta \approx 1$, which makes the LSP heavy enough to forbid the invisible Higgs decay. However, the recent XENON100 result on the direct detection of dark matter [8] excludes almost all the LSP mass region, although the LSP annihilation by the Higgs resonance effect can reduce the dark matter relic density significantly. For larger $\tan \beta$, the LSP gets lighter to open the Higgs invisible decay channel. In this case, the coupling between the Higgs boson and the LSP can be made small by a cancellation. Considering the charged Higgs boson mass bound from the LHC, the Higgs invisible decay branching fraction can be smaller than 0.1 for $\tan \beta \gtrsim 9$. For such a large $\tan \beta$, the NMSSM contribution to the Higgs boson mass becomes negligible. As the light singlino being the LSP couples very weakly to the quarks and leptons, its thermal relic density overcloses the universe. We will argue that the difficulties of the thermal LSP dark matter can be circumvented by a late-time entropy production of the saxion field inherent in the PQ-NMSSM, and the axion or the non-thermal LSP makes a good dark matter candidate. Analyzing the generic collider signatures of multi-jet and $h/W/Z$ plus missing energy for two chosen benchmark points with small and large $\tan \beta$, we find that a 5σ discovery can be achieved in the early stage of the 14 TeV LHC running.

This paper is organized as follows. In Sec. 2, we provide a general description of PQ-NMSSM. Then, we analyze the Higgs and the neutralino sectors of the minimal PQ-NMSSM. In Sec. 3, we study the phenomenology of a 125 GeV Higgs boson and a light

singlino to constrain the model parameter space from invisible decays of the Z and the Higgs boson, and the direct production of light neutralinos at LEP II. Analyzing the dark matter property of the LSP as a mixture of the singlino and Higgsino, the minimal model will be tightly constrained in Sec. 4. In Sec. 5, we analyze the collider signatures of the PQ-NMSSM at the LHC. We conclude in Sec. 6.

2 Peccei-Quinn Symmetric NMSSM

2.1 Model of PQ symmetry breaking

The $U(1)_{\text{PQ}}$ symmetry, which solves the strong CP problem of the standard model (SM), should be spontaneously broken between 10^9 and 10^{12} GeV. In SUSY models, it can be realized by introducing PQ charged but SM singlet chiral superfields

$$X_I = \phi_I + \sqrt{2}\theta\tilde{a}_I + \theta^2 F^{X_I}, \quad (2)$$

whose scalar components are stabilized at an intermediate scale, $\langle|\phi_I|\rangle \sim v_{\text{PQ}} \sim 10^9 - 10^{12}$ GeV. Then, the QCD axion corresponds to a linear combination of the axial components of ϕ_I . Such a large vacuum value, compared to the weak scale, can be easily obtained if $\langle|\phi_I|\rangle$ are determined by the interplay of soft SUSY breaking terms and the F -term scalar potential suppressed by a cut-off scale. In order to write down the higher dimensional term, we introduce two PQ-charged chiral superfields and the superpotential,

$$W_{\text{PQ}} = \frac{\kappa_{\text{PQ}}}{M_{\text{Pl}}} X_1^n X_2^{4-n} \quad (n = 1, 2), \quad (3)$$

where $M_{\text{Pl}} \simeq 2.4 \times 10^{18}$ GeV is the reduced Planck mass. The PQ symmetry is realized as

$$U(1)_{\text{PQ}} : X_1 \rightarrow e^{-iq_{X_1}\alpha} X_1, \quad X_2 \rightarrow e^{-iq_{X_2}\alpha} X_2, \quad (q_{X_1} + q_{X_2} = 4). \quad (4)$$

When one includes the soft SUSY breaking terms, the scalar potential is

$$\begin{aligned} V_{\text{PQ}} = & m_{X_1}^2 |\phi_1|^2 + m_{X_2}^2 |\phi_2|^2 + \left(\frac{A_{\text{PQ}} \kappa_{\text{PQ}}}{M_{\text{Pl}}} \phi_1^n \phi_2^{4-n} + \text{h.c.} \right) \\ & + \frac{\kappa_{\text{PQ}}^2}{M_{\text{Pl}}^2} (n^2 |\phi_1|^{2(n-1)} |\phi_2|^{2(4-n)} + (4-n)^2 |\phi_1|^{2n} |\phi_2|^{2(3-n)}). \end{aligned} \quad (5)$$

All the soft parameters $|m_{X_1}| \sim |m_{X_2}| \sim |A_{\text{PQ}}|$ are of the order of $m_{\text{soft}} = \mathcal{O}(10^2 - 10^3)$ GeV. In the case of $n = 2$, the additional \mathbb{Z}_2 symmetry ($X_I \rightarrow (-1)^I X_I$) is needed to prevent $M_X X_1 X_2$ term in the superpotential. The PQ symmetry breaking scale can be estimated as

$$v_{\text{PQ}} = \sqrt{\frac{1}{2} (q_X^2 \langle|\phi_1|^2\rangle + q_Y^2 \langle|\phi_2|^2\rangle)} \sim \langle|\phi_1|\rangle \sim \langle|\phi_2|\rangle \sim \sqrt{m_{\text{soft}} M_{\text{Pl}} / \kappa_{\text{PQ}}}, \quad (6)$$

and it is naturally lying on the axion window for a moderate value of κ_{PQ} . Non-zero auxiliary F -components of X_1 and X_2 are also developed. In canonical basis of the superfields, they are given as

$$\begin{aligned}\left\langle \frac{F^{X_1}}{\phi_1} \right\rangle &= -\left\langle \frac{1}{\phi_1} \frac{\partial W_{\text{PQ}}^*}{\partial \phi_1^*} \right\rangle = -\left\langle \frac{n W_{\text{PQ}}^*}{|\phi_1|^2} \right\rangle \sim \frac{\kappa_{\text{PQ}} v_{\text{PQ}}^2}{M_{\text{Pl}}} \sim m_{\text{soft}}, \\ \left\langle \frac{F^{X_2}}{\phi_2} \right\rangle &= -\left\langle \frac{1}{\phi_2} \frac{\partial W_{\text{PQ}}^*}{\partial \phi_2^*} \right\rangle = -\left\langle \frac{(4-n) W_{\text{PQ}}^*}{|\phi_2|^2} \right\rangle \sim \left\langle \frac{F^{X_1}}{\phi_1} \right\rangle \sim m_{\text{soft}}.\end{aligned}\quad (7)$$

After fixing the vacuum values, the scalar fields can be decomposed as $\phi_I = \langle |\phi_I| \rangle + (s_I + ia_I)/\sqrt{2}$. Masses of the PQ fields (s_I , a_I , and \tilde{a}_I) are generically of order of m_{soft} except the mass of the QCD axion $a_{\text{QCD}} = \sum_I q_I \langle |\phi_I| \rangle a_I / \sqrt{2} v_{\text{PQ}}$ of order $\sqrt{m_q \Lambda_{\text{QCD}}^3 / v_{\text{PQ}}}$, where m_q is a light quark mass. The PQ charged particles with masses of $\mathcal{O}(m_{\text{soft}})$ can play a important role in cosmology, which will be addressed in Sec. 4.

The axion solution to the strong CP problem can be realized by extending the Higgs sector through a superpotential term, $X_1^2 H_u H_d / M_{\text{Pl}}$ with $q_{H_u H_d} = -2q_{X_1}$ [2]. A simple consequence of this extension is that a bare Higgs-bilinear term is forbidden by the PQ symmetry and the right size of the μ -parameter is generated,

$$\mu_0 = \frac{\langle \phi_1^2 \rangle}{M_{\text{Pl}}} \sim \frac{v_{\text{PQ}}^2}{M_{\text{Pl}}} \sim m_{\text{soft}}. \quad (8)$$

The low energy theory after the PQ symmetry breaking could also be of the NMSSM type [4, 5] where the μ_0 term is extended to a scalar field S and the Higgs boson mass at 125-126 GeV could be realized with less fine-tuning. In the following subsection, we will describe how the PQ symmetry is incorporated into the NMSSM setup.

2.2 General PQ-NMSSM

In the NMSSM, the SM singlet superfield S couples to the Higgs fields with a renormalizable term $\lambda S H_u H_d$ in the superpotential. Then, S should have the PQ charge, $q_S = -q_{H_u H_d}$. Below the PQ symmetry breaking scale, the effective theory will be described by the general NMSSM:

$$W_{\text{eff}} = (\mu_0 + \lambda S) H_u H_d + \mu_S^2 S + \frac{1}{2} \mu'_S S^2 + \frac{1}{3} \kappa S^3, \quad (9)$$

where μ_0 , μ_S^2 , μ'_S , and κ are the effective parameters determined by interactions between S and X_I . Obviously, they should be vanishing in the PQ symmetric limit, $v_{\text{PQ}} \rightarrow 0$. In order for S to be a light degree of freedom that survives around TeV scale, μ_0 , μ_S , $\mu'_S \lesssim \mathcal{O}(m_{\text{soft}})$, and corresponding soft SUSY breaking parameters are around m_{soft} as well. It is expected that sizable values of μ_S^2 and μ'_S can be obtained by the PQ symmetry breaking model. We

will study explicitly how such PQ symmetry breaking parameters can be generated for the models given in Sec. 2.1.

For the PQ symmetry breaking model (3) with $n = 1$ ($W_{\text{PQ}} = \kappa_{\text{PQ}} XY^3/M_{\text{Pl}}$), the relevant PQ invariant superpotential is

$$W = \left(\frac{X_1^2}{M_{\text{Pl}}} + \lambda S \right) H_u H_d + \dots, \quad (10)$$

where dots denote highly suppressed terms that do not contribute to the Higgs phenomenology. The non-trivial μ_S^2 can be obtained from a PQ invariant higher dimensional term in the Kähler potential,

$$K = \frac{\kappa_{XS}}{M_{\text{Pl}}} X_1^{*2} S + \text{h.c.} \quad (11)$$

At low energy, κ_{XS} and X_I can be regarded as SUSY breaking spurion superfields with $\kappa_{XS} = \kappa_0 + \theta^2 \kappa_F m_{\text{soft}} + \bar{\theta}^2 \kappa_{\bar{F}} m_{\text{soft}} + \theta^2 \bar{\theta}^2 \kappa_D m_{\text{soft}}^2$, and $X_I = \langle \phi_I \rangle (1 + \theta^2 \langle F^{X_I} / \phi_I \rangle)$. κ_0 , κ_F , $\kappa_{\bar{F}}$, κ_D are all $\mathcal{O}(1)$ constants with a reasonable assumption that they and the soft SUSY breaking terms for the superpartners of the SM fields have the same origin. Then, by (6) and (7),

$$\mu_S^2 = \left(\kappa_{\bar{F}} m_{\text{soft}} + 2 \left\langle \frac{F^{X_1^*}}{\phi_1^*} \right\rangle \right) \left(\frac{\langle \phi_1^{*2} \rangle}{M_{\text{Pl}}} \right) \sim \left(\frac{v_{\text{PQ}}^2}{M_{\text{Pl}}} \right)^2 \sim m_{\text{soft}}^2, \quad (12)$$

but still μ'_S and κ are suppressed. Note that the superpotential term $X_1^2 H_u H_d / M_{\text{Pl}}$ in (10) can be removed by the holomorphic field redefinition $S \rightarrow S - X_1^2 / \lambda M_{\text{Pl}}$ without loss of generality. Then, the low energy effective superpotential corresponds to the minimal type of PQ-NMSSM [9],

$$W_{\text{eff}} = \lambda S H_u H_d + \mu_S^2 S. \quad (13)$$

As for the model with $n = 2$ ($W_{\text{PQ}} = \kappa_{\text{PQ}} X^2 Y^2 / M_{\text{Pl}}$), the same superpotential (10) and Kähler potential (11) are allowed so that the sizable μ_0 , μ_S^2 are generated. As discussed in Sec. 2.1, there is an additional \mathbb{Z}_2 symmetry $X_I \rightarrow (-1)^I X_I$, $S \rightarrow -S$, $H_u H_d \rightarrow -H_u H_d$ at renormalizable level, in order to insure that terms like $X_1 X_2$, $X_2^2 S$ are absent. Since the \mathbb{Z}_2 symmetry is explicitly broken by the term $X_1^2 H_u H_d / M_{\text{Pl}}$, a cosmologically dangerous domain wall is not produced. Besides, the \mathbb{Z}_2 breaking tadpole induced by supergravity loop corrections are suppressed due to the PQ symmetry. This model is more complicated than the model with $n = 1$. However, a sizable μ'_S term can be generated if there are matter superfields Z_1 , Z_2 whose masses are given by $\langle |\phi_1| \rangle$ from a superpotential term $X_1 Z_1 Z_2$ with the PQ charges $q_{Z_1} = 3q_{X_1}$, $q_{Z_2} = -4q_{X_1}$. Under the \mathbb{Z}_2 symmetry, $Z_I \rightarrow (-1)^I Z_I$. Then, the following superpotentials are allowed

$$\Delta W = \lambda_{XZ} X_1 Z_1 Z_2 + \lambda_{ZS} Z_2 S^2 + \frac{1}{M_{\text{Pl}}} \left(\kappa_{XZ} X_2^3 Z_1 + \kappa_{XZS} X_1^2 Z_2 S \right) + \frac{\lambda_{XS}}{M_{\text{Pl}}^2} X_2^4 S + \dots \quad (14)$$

Since the masses of Z_1 and Z_2 are of the order of v_{PQ} , they should be integrated out, at the PQ symmetry breaking scale, by the superfield equations of motion:

$$\frac{\partial W}{\partial Z_1} \simeq \frac{\partial W}{\partial Z_2} \simeq 0. \quad (15)$$

By substituting the solutions of (15) to Z_I of (14), $\Delta\mu_S^2$ and μ'_S are generated as

$$\begin{aligned} \Delta\mu_S^2 &= \left(\frac{\kappa_{XZS}\kappa_{XZ}\langle\phi_1\rangle}{\lambda_{XZ}\langle\phi_2\rangle} + \lambda_{XS} \right) \left(\frac{\langle\phi_2^2\rangle}{M_{\text{Pl}}} \right)^2 \sim \left(\frac{v_{\text{PQ}}^2}{M_{\text{Pl}}} \right)^2 \sim m_{\text{soft}}^2, \\ \mu'_S &= \left(\frac{\lambda_{ZS}\kappa_{XZ}\langle\phi_2\rangle}{\lambda_{XZ}\langle\phi_1\rangle} \right) \left(\frac{\langle\phi_2^2\rangle}{M_{\text{Pl}}} \right) \sim \frac{v_{\text{PQ}}^2}{M_{\text{Pl}}} \sim m_{\text{soft}}. \end{aligned} \quad (16)$$

This case corresponds to the singlet extension of the MSSM [10],

$$W_{\text{eff}} = (\mu_0 + \lambda S)H_u H_d + \mu_S^2 S + \mu'_S S^2, \quad (17)$$

while κ is still suppressed. This is a generic consequence of the PQ extension of the NMSSM.

The PQ sector contributions to the soft SUSY-breaking parameters for Higgs and singlet sector are coming from θ^2 ($\bar{\theta}^2$) component of the spurion superfields $X_I = \langle\phi_I\rangle(1 + \theta^2\langle F^{X_I}/\phi_I\rangle)$ (X_I^*), which are the same order of the MSSM soft SUSY-breaking parameters, m_{soft} .

2.3 Minimal PQ-NMSSM

In this subsection, we investigate the phenomenological consequences of the minimal PQ-NMSSM [4] whose low-energy effective superpotential takes the form of (13) in addition to the usual MSSM Yukawa superpotential terms. The new superfield S is singlet under the SM gauge group, and it can acquire the vacuum expectation value (VEV) to give the natural size of the μ term of the electroweak (EW) scale.

2.3.1 Higgs sector

Here, we describe the Higgs scalar potential, its vacuum structure, and the mass spectra around the vacuum. The Higgs scalar potential consists of the following F - and D -term contributions from the superpotential (13), and soft SUSY-breaking terms,

$$V_F = |\lambda(H_u^+ H_d^- - H_u^0 H_d^0) + \mu_S^2|^2 + \lambda^2 |S|^2 (|H_u^0|^2 + |H_u^+|^2 + |H_d^0|^2 + |H_d^-|^2), \quad (18)$$

$$V_D = \frac{g_1^2 + g_2^2}{8} (|H_u^0|^2 + |H_u^+|^2 - |H_d^0|^2 - |H_d^-|^2)^2 + \frac{g_2^2}{2} |H_u^+ H_d^{0*} + H_u^0 H_d^{-*}|^2, \quad (19)$$

$$\begin{aligned} V_S &= m_{H_u}^2 (|H_u^0|^2 + |H_u^+|^2) + m_{H_d}^2 (|H_d^0|^2 + |H_d^-|^2) + m_S^2 |S|^2 \\ &\quad + [\lambda A_\lambda (H_u^+ H_d^- - H_u^0 H_d^0) S + t_S S + \text{h.c.}]. \end{aligned} \quad (20)$$

We assume that all the coefficients in the potentials are real so that any explicit CP violation does not occur other than the Cabibbo-Kobayashi-Maskawa phase. The VEVs of the charged Higgs field should be vanishing in order to obtain a successful EW symmetry breaking minimum. One of the VEVs of the charged Higgs field, e.g., $\langle H_u^+ \rangle$ can be made zero with positive $\langle H_u^0 \rangle = v_u$ by the $SU(2)$ gauge choice. The other one, however, is not guaranteed to vanish in contrast to the MSSM case in which the minimization condition $\partial V / \partial H_u^+ = 0$ gives $\langle H_d^- \rangle = 0$. Still, it can be shown that $\langle H_d^- \rangle = 0$ satisfies the extremum conditions and it will turn out to be local minimum if all masses squared of the charged Higgs sector are non-negative. Therefore, it is reasonable to assume that $\langle H_d^- \rangle = 0$ and the charged Higgs boson masses squared are required to be positive. The Higgs potential can then be written as

$$V_{\text{Higgs}} = (m_{H_u}^2 + \lambda^2 |S|^2) |H_u^0|^2 + (m_{H_d}^2 + \lambda^2 |S|^2) |H_d^0|^2 - [\lambda(A_\lambda S + \mu_S^2) H_u^0 H_d^0 + \text{h.c.}] \\ + \frac{g_1^2 + g_2^2}{8} (|H_u^0|^2 - |H_d^0|^2)^2 + \lambda^2 |H_u^0 H_d^0|^2 + m_S^2 |S|^2 + [t_S S + \text{h.c.}] + \mu_S^4. \quad (21)$$

Expanding the neutral Higgs fields around their VEVs, one gets

$$H_u^0 = v_u + \frac{H_{uR} + iH_{uI}}{\sqrt{2}}, \quad (22)$$

$$H_d^0 = v_d + \frac{H_{dR} + iH_{dI}}{\sqrt{2}}, \quad (23)$$

$$S = v_S + \frac{S_R + iS_I}{\sqrt{2}}. \quad (24)$$

In general, the VEVs of the neutral Higgs fields can have non-trivial phases that induce the spontaneous CP violation. However, as shown in [11], there cannot be such spontaneous CP violation in the minimal PQ-NMSSM since the extrema with non-trivial phases are local maxima rather than minima. Accordingly, one can always set the VEVs of the neutral Higgs fields to be real. The equations of motion $\partial V_{\text{Higgs}} / \partial H_u^0 = \partial V_{\text{Higgs}} / \partial H_d^0 = \partial V_{\text{Higgs}} / \partial S = 0$ at the vacuum are

$$m_{H_u}^2 + \mu_{\text{eff}}^2 + \lambda^2 v_d^2 + \frac{g_1^2 + g_2^2}{4} (v_u^2 - v_d^2) - b_{\text{eff}} / \tan \beta = 0, \quad (25)$$

$$m_{H_d}^2 + \mu_{\text{eff}}^2 + \lambda^2 v_u^2 + \frac{g_1^2 + g_2^2}{4} (v_d^2 - v_u^2) - b_{\text{eff}} \tan \beta = 0, \quad (26)$$

$$v_S [m_S^2 + \lambda^2 v^2] + t_S - \lambda A_\lambda v_u v_d = 0, \quad (27)$$

where $\tan \beta \equiv v_u / v_d$, $v^2 \equiv v_u^2 + v_d^2$, $\mu_{\text{eff}} \equiv \lambda v_S$, and $b_{\text{eff}} \equiv \mu_{\text{eff}} A_\lambda + \lambda \mu_S^2$. These three minimization equations can also be cast into the following form,

$$\sin 2\beta = \frac{2b_{\text{eff}}}{2\mu_{\text{eff}}^2 + m_{H_u}^2 + m_{H_d}^2 + \lambda^2 v^2}, \quad (28)$$

$$\frac{1}{2} m_Z^2 = \frac{m_{H_d}^2 - m_{H_u}^2 \tan^2 \beta}{\tan^2 \beta - 1} - \mu_{\text{eff}}^2, \quad (29)$$

$$v_S = \frac{\lambda A_\lambda v^2 \sin 2\beta - 2t_S}{2(m_S^2 + \lambda^2 v^2)}, \quad (30)$$

where $g^2 \equiv (g_1^2 + g_2^2)/2$ and $v \simeq 174$ GeV. In general, there can be false vacua that do not satisfy the proper EW vacuum conditions, i.e. $v^2 \simeq (174 \text{ GeV})^2$, $v_u, v_d, v_S \neq 0$, $\tan \beta \neq 1$. For the EW vacuum to be stable, the false vacua should not be deeper than the EW vacuum or distant enough to take a longer time to decay than the age of the Universe. Finding such conditions, however, would be in need of systematic studies as carried out in [12], which consider the case of the \mathbb{Z}_3 -invariant NMSSM. Although such extensive works in the case of the PQ-NMSSM are beyond the scope of this paper, we here leave a comment on the simplest condition for the false vacuum with $v_u = v_d = 0$, $v_S \neq 0$.¹ For this false vacuum, the minimum value of the potential is given as

$$V_{\text{F},\text{min}} = -\frac{t_S^2}{m_S^2} + \mu_S^4. \quad (31)$$

On the other hand, the potential value at the EW minimum is

$$V_{\text{T},\text{min}} = -\lambda^2 \frac{m_Z^4 \sin^2 2\beta}{4g^4} - \frac{m_Z^4 \cos^2 2\beta}{4g^4} + \frac{2\mu_{\text{eff}}}{\lambda} t_S + \frac{1}{\lambda^2} m_S^2 \mu_{\text{eff}}^2 + \mu_S^4. \quad (32)$$

And, if one imposes the condition that $V_{\text{T},\text{min}} \leq V_{\text{F},\text{min}}$, it can be shown that this is always satisfied for $|t_S| \gg |A_\lambda|v^2$. The large negative t_S value will make the singlet scalar heavy enough to be decoupled as can be seen in (27). Therefore, in the following sections for the phenomenological analysis, we confine the parameter space to the large $-t_S \sim \mathcal{O}(\text{TeV})^3$.

We now expand the Higgs scalar potential around the EW vacuum. By collecting quadratic terms and eliminating the soft mass terms through the minimization equations, we get, for the CP-even Higgs fields in the (H_{dR}, H_{uR}, S_R) basis,

$$\mathcal{M}_S^2 = \begin{pmatrix} m_Z^2 \cos^2 \beta + m_A^2 \sin^2 \beta & (2\lambda^2 v^2 - m_A^2 - m_Z^2) \sin \beta \cos \beta & \lambda v (2\mu_{\text{eff}} \cos \beta - A_\lambda \sin \beta) \\ m_Z^2 \sin^2 \beta + m_A^2 \cos^2 \beta & & \lambda v (2\mu_{\text{eff}} \sin \beta - A_\lambda \cos \beta) \\ & m_S^2 + \lambda^2 v^2 & \end{pmatrix}, \quad (33)$$

where $m_A^2 \equiv 2b_{\text{eff}}/\sin 2\beta$. Upon diagonalizing the matrix, one eventually obtains the following tree-level lightest Higgs boson mass in the limit of $m_A \gg m_Z$ and $m_S \gg \mu_{\text{eff}}, A_\lambda$.

$$m_{h,\text{tree}}^2 \simeq m_Z^2 \cos^2 2\beta + \lambda^2 v^2 \left(\sin^2 2\beta - \frac{(2\mu_{\text{eff}} - A_\lambda \sin 2\beta)^2}{m_S^2} \right). \quad (34)$$

The second and third terms proportional to λ^2 come from the NMSSM Yukawa coupling $\lambda S H_u H_d$ in the superpotential, which can significantly enhance the tree-level lightest Higgs

¹A numerical analysis based on some analytic conditions would be needed in the other cases that can be analytically investigated.

boson mass compared to the MSSM. The second term is due to the doublet scalar quartic coupling $\lambda^2 |H_u^0 H_d^0|^2$ and is sensitively becoming small for the large $\tan \beta$ ($\sin 2\beta \sim 2/\tan \beta$), while the third term is from the doublet-singlet mixing and $\lambda^2 |S|^2 |H_{u,d}^0|^2$ terms in the scalar potential.

For the CP-odd Higgs fields,

$$\mathcal{M}_P^2 = \begin{pmatrix} m_A^2 \sin^2 \beta & m_A^2 \sin \beta \cos \beta & \lambda v A_\lambda \sin \beta \\ & m_A^2 \cos^2 \beta & \lambda v A_\lambda \cos \beta \\ & & m_S^2 + \lambda^2 v^2 \end{pmatrix} \quad (35)$$

in the (H_{dI}, H_{uI}, S_I) basis. After dropping the Goldstone mode obtained by rotating the upper 2×2 matrix, the following mass matrix appears in the (A, S_I) basis,

$$\mathcal{M}_{P'}^2 = \begin{pmatrix} m_A^2 & \lambda v A_\lambda \\ \lambda v A_\lambda & m_S^2 + \lambda^2 v^2 \end{pmatrix}. \quad (36)$$

The corresponding mass eigenvalues are

$$m_{A_0, A_1, \text{tree}}^2 = \frac{1}{2} \left(m_A^2 + m_S^2 + \lambda^2 v^2 \mp \sqrt{(m_S^2 - m_A^2 + \lambda^2 v^2)^2 + 4\lambda^2 v^2 A_\lambda^2} \right). \quad (37)$$

For the charged Higgs fields,

$$\mathcal{M}_\pm^2 = (m_A^2 + m_W^2 - \lambda^2 v^2) \begin{pmatrix} \cos^2 \beta & \cos \beta \sin \beta \\ \cos \beta \sin \beta & \sin^2 \beta \end{pmatrix} \quad (38)$$

in the (H_u^+, H_d^{-*}) basis. By rotating the matrix by the angle $\pi/2 - \beta$, one can obtain the Goldstone mode and a mass eigenstate with the mass eigenvalue,

$$m_{H^\pm, \text{tree}}^2 = m_A^2 + m_W^2 - \lambda^2 v^2. \quad (39)$$

All the above masses will receive important loop corrections (see Appendix C in [3]). For the analysis in Secs. 3 and 5, we include the loop contributions as implemented in the NMSSMTOOLS 3.1.0 [13]²

2.3.2 Neutralino sector

The singlet superfield S in the NMSSM also significantly changes the neutralino sector compared with the MSSM. The additional singlino field \tilde{S} mixes with the neutral Higgsinos

² The current version of the NMSSMTOOLS implements only the \mathbb{Z}_3 -invariant NMSSM. We used modified codes for adapting to the case of the PQ-NMSSM.

$\tilde{H}_d^0, \tilde{H}_u^0$ and the gauginos $\tilde{\lambda}_1, \tilde{\lambda}_2^3$, producing a symmetric 5×5 mass matrix $M_{\tilde{\chi}^0}$,

$$\mathcal{M}_{\tilde{\chi}^0} = \begin{pmatrix} M_1 & 0 & -g_1 v_d / \sqrt{2} & g_1 v_u / \sqrt{2} & 0 \\ & M_2 & g_2 v_d / \sqrt{2} & -g_2 v_u / \sqrt{2} & 0 \\ & & 0 & -\mu_{\text{eff}} & -\lambda v_u \\ & & & 0 & -\lambda v_d \\ & & & & 0 \end{pmatrix} \quad (40)$$

in the basis $(-i\tilde{\lambda}_1, -i\tilde{\lambda}_2^3, \tilde{H}_d^0, \tilde{H}_u^0, \tilde{S})$. The diagonalization of this mass matrix and resulting mixing matrices are computed in Appendix A. An important point to note is that there is no SUSY mass term for the singlino \tilde{S} in the minimal PQ-NMSSM. The singlino-like neutralino mass is induced only by mixing, and thus making the corresponding mass eigenvalue generically quite small. The lightest neutralino mass appears to be

$$\begin{aligned} m_{\tilde{\chi}_1^0} &= -2(\mu_{\text{eff}} N_{13} N_{14} + \lambda v \cos \beta N_{14} N_{15} + \lambda v \sin \beta N_{13} N_{15}) \\ &\quad + \sqrt{2} v (g_1 N_{11} - g_2 N_{12}) (-N_{13} \cos \beta + N_{14} \sin \beta) + M_1 N_{11}^2 + M_2 N_{12}^2 \\ &\simeq \frac{\lambda^2 v^2}{\mu_{\text{eff}}} \left[\sin 2\beta - \frac{\lambda^2 v^2}{\mu_{\text{eff}}^2} \sin 2\beta - \left(\frac{g_1^2 v^2}{2\mu_{\text{eff}} M_1} + \frac{g_2^2 v^2}{2\mu_{\text{eff}} M_2} \right) \cos^2 2\beta + \mathcal{O}\left(\frac{v^4}{\mu_{\text{eff}}^4}\right) \right] \end{aligned} \quad (41)$$

when $M_1, M_2 \sim \mu_{\text{eff}} \gg \lambda v$. Here, N_{1i} 's denote the neutralino mixing components given in Appendix A. The larger $\tan \beta$ makes the lightest neutralino mass smaller. Moreover, one can see that the lightest neutralino becomes lighter as μ_{eff} increases. It can also be easily checked that the mass becomes zero as μ_{eff} vanishes if we consider decoupling of the gauginos, i.e., $M_1, M_2 \gg \mu_{\text{eff}}, \lambda v$. This observation implies that there must exist a maximum value of the lightest neutralino mass at a certain value of μ_{eff} for a fixed value of λv in decoupling limit of the gauginos. We can find that the upper bound of the lightest neutralino mass is given by

$$m_{\tilde{\chi}_1^0} = \lambda v \cos \beta \quad \text{at } \mu_{\text{eff}} = \lambda v \sin \beta \quad (42)$$

for $\tan \beta > 1$, which gives $m_{\tilde{\chi}_1^0} \lesssim 85 \text{ GeV}$ for $\lambda = 0.7$.

3 Higgs phenomenology of the PQ-NMSSM

In this section, we discuss the Higgs phenomenology of the PQ-NMSSM in the light of the recent ATLAS and CMS discovery of a 125 GeV Higgs boson. We will show viable parameter spaces that can give the presumed Higgs boson mass without conflicting any existing phenomenological constraints, and discuss their feasibility from the point of view of naturalness.

As discussed in Sec. 2.3.1, the relevant parameters for the Higgs sector are $\lambda, \tan \beta, \mu_{\text{eff}}, m_A$ (or A_λ), μ_S^2 , and t_S . For μ_S^2 , we take a weak scale value of $\mathcal{O}(100 \text{ GeV})^2$ since it

affects the Higgs sector only via the b_{eff} ($= \mu_{\text{eff}}A_\lambda + \lambda\mu_S^2$) term so that the variations of μ_{eff} or $m_A(A_\lambda)$ include its effect. For m_A and t_S , we select their proper values that can give $m_S^2 \gg m_A^2 \gg m_Z^2$ in order to make the tree-level Higgs boson mass as large as possible according to (34).³ A large value of λ is needed to increase the Higgs boson mass through the specific contribution of the NMSSM. However, an investigation into the scale of the perturbativity breaking by λ driven by renormalization group running should be preceded to avoid the scale being lower than the PQ scale of $10^9 - 10^{12}$ GeV. It can be shown that the perturbativity breaking scale decreases rapidly as $\tan\beta$ becomes small. In Table 1, we show the perturbativity breaking scales in the small $\tan\beta$ region for a fixed value of $\lambda = 0.7$, which is a marginal choice for the PQ-NMSSM to be viable in the small $\tan\beta$ region.

Table 1: Perturbativity breaking scale Λ for $\tan\beta \lesssim 2$.

$\tan\beta$	1.1	1.2	1.3	1.4	1.5	1.7	1.9
Λ (GeV)	10^{10}	10^{11}	10^{12}	10^{13}	10^{14}	10^{15}	10^{16}

One of the most important features of the PQ-NMSSM is that the lightest neutralino is relatively lighter than that of the MSSM. Such a light neutralino can raise conflicts with several phenomenological constraints. Furthermore, since the neutralino sector shares some parameters with the Higgs sector, the constraints can also place serious restrictions on the viable parameter space for the 125 GeV Higgs signals. As for the neutralino sector, the relevant parameters are λ , $\tan\beta$, μ_{eff} , M_1 , and M_2 as can be seen in Sec. 2.3.2. Among them, the overlapping parameters with the Higgs sector are λ , $\tan\beta$, and μ_{eff} . The phenomenological constraints on the light neutralino come from

- I. Z invisible decay ($Z \rightarrow \tilde{\chi}_1^0 \tilde{\chi}_1^0$),
- II. $\tilde{\chi}_1^0 \tilde{\chi}_2^0$ production at LEP II ($e^+e^- \rightarrow \tilde{\chi}_1^0 \tilde{\chi}_2^0$),
- III. Higgs invisible decay ($h \rightarrow \tilde{\chi}_1^0 \tilde{\chi}_1^0$).

These constraints impose additional restrictions on the parameter space of $\tan\beta$ and μ_{eff} . In particular, the constraints I and III motivate us to consider two scenarios according to the value of $\tan\beta$. For small $\tan\beta \lesssim 1.6$, the lightest neutralino turns out to be heavier than the half of the 125 GeV Higgs mass so that the constraints I and III are satisfied by

³ The region of $m_A^2 \sim m_Z^2$ will also be considered in the subsequent discussion with regard to the suppression of the ratio of the Higgs invisible decay. However, it will turn out to be unfavorable to the constraint on the charged Higgs boson.

kinematics. For large $\tan\beta \gtrsim 1.6$, however, it should be considered a non-trivial mechanism of suppressing the Higgs invisible decay.

For our study with specific choices of the usual MSSM parameters, the gluino mass parameter M_3 is taken to be 1 TeV, which is above the region ruled out by current search results [14], while being able to be accessed in the LHC experiment. For the same purpose, we set the first two generation squarks at ~ 2 TeV. In regard to the remaining gaugino mass parameters, M_1 and M_2 , we consider two kinds of scenarios, the grand unification theory (GUT) relation of the gaugino masses and the unified gaugino masses in the TeV scale mirage mediation [15],

$$\text{GUT : } 6M_1 = 3M_2 = M_3 = 1 \text{ TeV}, \quad (43)$$

$$\text{TeV mirage : } M_1 = M_2 = M_3 = 1 \text{ TeV}. \quad (44)$$

In the case of the GUT relation, the lightest neutralino becomes generically lighter than in the case of decoupled heavy EW gauginos since the light EW gauginos can have a mixing with the Higgsino and the singlino. Furthermore, the mixing can deliver important phenomenological consequences through affecting the coupling of Higgs to the lightest neutralino pair as to be discussed in the following subsections. On the other hand, in the case of the TeV mirage, the EW gauginos are heavy enough so that the relation (42) holds to give heavier lightest neutralino, and the lightest neutralino is almost composed of Higgsino and singlino.

In Subsecs. 3.1 and 3.2, we review the constraints I, II, and III in the case of the light neutralino. We then proceed to analyze two scenarios depending on $\tan\beta$ in Subsecs. 3.3.1 and 3.3.2.

3.1 LEP II constraints on light neutralino

In the PQ-NMSSM, not only the lightest singlino-like neutralino $\tilde{\chi}_1^0$ but also the next-to-lightest neutralino $\tilde{\chi}_2^0$ can be light enough to get constrained by the Z invisible decay and/or the direct production in the e^+e^- scattering of the LEP II experiment through the processes shown in Fig. 1.

The Z boson decay rate to a lightest-neutralino pair is given by

$$\Gamma(Z \rightarrow \tilde{\chi}_1^0 \tilde{\chi}_1^0) = \frac{g_2^2}{4\pi} \frac{(N_{13}^2 - N_{14}^2)^2}{24 \cos^2 \theta_W} m_Z \left[1 - \left(\frac{2M_{\tilde{\chi}_1^0}}{m_Z} \right)^2 \right]^{3/2}, \quad (45)$$

where N_{1i} 's are neutralino mixing components shown explicitly in Appendix A. From the constraint on the Z invisible decay, $\Gamma_{\text{inv}} < 3 \text{ MeV}$ [16], we find that

$$|N_{13}^2 - N_{14}^2| \lesssim 0.13. \quad (46)$$

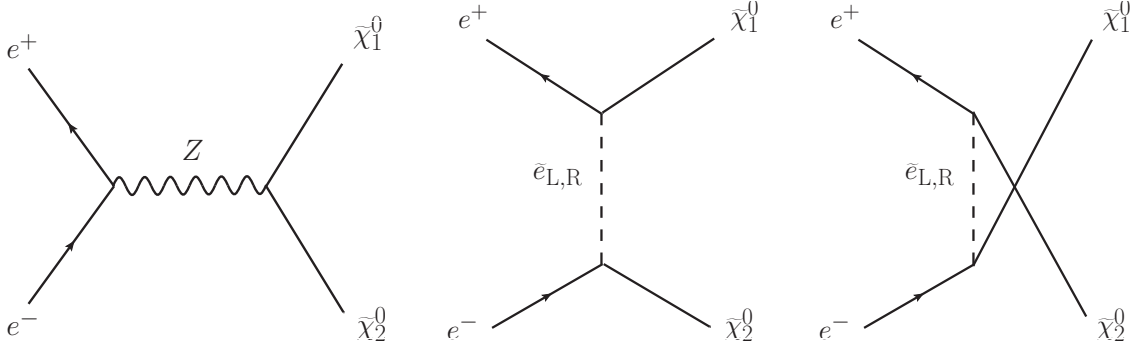


Figure 1: Feynman diagrams for the neutralino production $e^+e^- \rightarrow \tilde{\chi}_1^0 \tilde{\chi}_2^0$

In the LEP II experiment, the next-to-lightest neutralino can be produced in association with the lightest neutralino as in Fig. 1. If one assumes that the sleptons are much heavier than the Z boson, the slepton exchange diagrams can be neglected in the LEP II experiment. Then, the production cross section is given as

$$\begin{aligned}
& \sigma(e^+e^- \rightarrow Z^* \rightarrow \tilde{\chi}_1^0 \tilde{\chi}_2^0) \\
&= \frac{1}{96\pi} \frac{g_2^2}{\cos^4 \theta_W} \left(\frac{1}{4} - \sin^2 \theta_W + 2 \sin^4 \theta_W \right) (N_{13}N_{23} - N_{14}N_{24})^2 \frac{s}{(s - m_Z^2)^2} \\
& \times \left[1 - \frac{2(M_{\tilde{\chi}_1^0}^2 + M_{\tilde{\chi}_2^0}^2)}{s} + \frac{(M_{\tilde{\chi}_2^0}^2 - M_{\tilde{\chi}_1^0}^2)^2}{s^2} \right]^{1/2} \\
& \times \left[1 - \frac{6M_{\tilde{\chi}_1^0}M_{\tilde{\chi}_2^0} + (M_{\tilde{\chi}_1^0}^2 + M_{\tilde{\chi}_2^0}^2)}{2s} - \frac{(M_{\tilde{\chi}_2^0}^2 - M_{\tilde{\chi}_1^0}^2)^2}{2s^2} \right].
\end{aligned} \tag{47}$$

The production cross section is given upper bounds depending on the masses of the neutralinos by the OPAL analysis result [17]. In the case that the lightest neutralino is nearly massless, the most conservative bound is given as follows.

$$\sigma(e^+e^- \rightarrow \tilde{\chi}_1^0 \tilde{\chi}_2^0) < 10 \text{ fb} \tag{48}$$

with $\text{Br}(\tilde{\chi}_2^0 \rightarrow Z\tilde{\chi}_1^0) = 1$. However, such an upper limit of the production cross section can be moderated in the case that the lightest neutralino is heavier. This will be discussed in more detail in Subsec. 3.3.1.

3.2 Higgs invisible decay

The light neutralino states can also induce the invisible decay of the Higgs boson. If there exists substantial invisible decay ratio of the Higgs boson, the visible decay modes such $h \rightarrow \gamma\gamma$ or $h \rightarrow WW/ZZ$ will be significantly reduced. As this would make it difficult to explain the recent discovery of the 125 GeV Higgs boson signal in the ATLAS and CMS

experiments, it is of particular importance to consider the Higgs invisible decay in the plausible parameter space.

The invisible decay of the lightest CP-even Higgs boson is determined by the Higgs-neutralino coupling shown in Appendix C,

$$g_{h\tilde{\chi}_i^0\tilde{\chi}_j^0} = \frac{\lambda}{\sqrt{2}}(S_{11}\Pi_{ij}^{45} + S_{12}\Pi_{ij}^{35} + S_{13}\Pi_{ij}^{34}) + \frac{g_1}{2}(S_{11}\Pi_{ij}^{13} - S_{12}\Pi_{ij}^{14}) - \frac{g_2}{2}(S_{11}\Pi_{ij}^{23} - S_{12}\Pi_{ij}^{24}), \quad (49)$$

where $\Pi_{ij}^{ab} \equiv N_{ia}N_{jb} + N_{ib}N_{ja}$. Here, S_{ab} and N_{ij} are the CP-even Higgs mixing matrix and the neutralino mixing matrix, respectively. As analyzed in Appendix A including the first, second, and dominant third-order contributions, the mixing components in the neutralino mass matrix are

$$N_{11} \simeq -\frac{g_1\lambda v^2 \cos 2\beta}{\sqrt{2}M_1\mu_{\text{eff}}}, \quad (50)$$

$$N_{12} \simeq \frac{g_2\lambda v^2 \cos 2\beta}{\sqrt{2}M_2\mu_{\text{eff}}}, \quad (51)$$

$$N_{13} \simeq -\frac{\lambda v \cos \beta}{\mu_{\text{eff}}} - \frac{\lambda v^3}{2\mu_{\text{eff}}^2} \left(\frac{g_1^2}{M_1} + \frac{g_2^2}{M_2} \right) \cos 2\beta \sin \beta + \frac{3\lambda^3 v^3}{\sqrt{2}\mu_{\text{eff}}^3} \sin 2\beta \sin \beta, \quad (52)$$

$$N_{14} \simeq -\frac{\lambda v \sin \beta}{\mu_{\text{eff}}}, \quad (53)$$

$$N_{15} \simeq 1. \quad (54)$$

We here include only the leading term for each component except N_{13} , for which the second and third terms in (52) can be sizable when $\tan \beta \gtrsim (\mu/\lambda v)^2$. By putting these terms into (49), one can find $g_{h\tilde{\chi}_1^0\tilde{\chi}_1^0}$ for the coupling between the lightest CP-even Higgs and a lightest-neutralino pair. In the limiting case of vanishing doublet-singlet mixing in the Higgs sector, i.e., $S_{13} = 0$, the coupling is given by

$$\begin{aligned} \frac{g_{h\tilde{\chi}_1^0\tilde{\chi}_1^0}}{S_{12}} &\simeq -\frac{\sqrt{2}\lambda^2 v}{\mu_{\text{eff}}} \left(1 + c \frac{3m_W^2}{2M_2\mu^2} \right) \left(1 - \frac{3\sqrt{2}\lambda^2 v^2}{\mu_{\text{eff}}^2} \right) \frac{1}{\tan \beta} \\ &\quad - \frac{\sqrt{2}\lambda^2 v}{\mu_{\text{eff}}} \left(c - c \frac{9m_W^4}{4M_2^2\mu_{\text{eff}}^2} - \frac{3m_W^2}{M_2\mu_{\text{eff}}} \right), \end{aligned} \quad (55)$$

where $c \equiv S_{11}/S_{12}$ and $g_2 \simeq 2g_1$. It was assumed that the GUT relation for the gaugino masses, $M_2 = 2M_1$, and applied a crude approximation, $\sin \beta \simeq 1$, $\cos \beta \simeq 1/\tan \beta$, $\sin 2\beta \simeq 2/\tan \beta$ and $\cos 2\beta \simeq 1$ for $\tan \beta \gtrsim 3$ to derive the above relation. Note that the coefficient c corresponds to $-\tan \alpha$ ($-\pi/2 \leq \alpha \leq 0$) in the MSSM limit, where α is the CP-even Higgs mixing angle in the MSSM. For making this coupling vanishing, we find a relation,

$$\frac{1}{\tan \beta} \simeq - \left(c - c \frac{9m_W^4}{4M_2^2\mu_{\text{eff}}^2} - \frac{3m_W^2}{M_2\mu_{\text{eff}}} \right) \left(1 - c \frac{3m_W^2}{2M_2\mu_{\text{eff}}} \right) \left(1 + \frac{3\sqrt{2}\lambda^2 v^2}{\mu_{\text{eff}}^2} \right)$$

$$= \left[\frac{3m_W^2}{M_2\mu_{\text{eff}}} - c \left(1 + \frac{9m_W^4}{4M_2^2\mu_{\text{eff}}^2} \right) - c^2 \frac{3m_W^2}{2M_2\mu_{\text{eff}}} \left(1 - \frac{9m_W^4}{4M_2^2\mu_{\text{eff}}^2} \right) \right] \left(1 + \frac{3\sqrt{2}\lambda^2 v^2}{\mu_{\text{eff}}^2} \right). \quad (56)$$

For $M_2\mu_{\text{eff}} \gg m_W^2$, the coefficients of c and c^2 are always positive, so the larger c requires the larger value of $\tan\beta$. The effect of the Higgs mixing c will be discussed in Subsec. 3.3.2.

3.3 Phenomenology depending on $\tan\beta$

3.3.1 $1 \lesssim \tan\beta \lesssim 2$: heavy neutralino scenario

We now discuss the possibility for the small $1 \lesssim \tan\beta \lesssim 2$ region. Such small $\tan\beta$ makes singlino-Higgsino mixing large and thus the lightest neutralino heavy. One can obtain the mass of the lightest neutralino larger than $m_h/2$ in order to forbid kinematically the invisible decays of the Z boson and the Higgs boson. In this case, however, it may concern the $\tilde{\chi}_1^0\tilde{\chi}_2^0$ pair production as the next-to-lightest neutralino can also be light enough. As discussed in Sec. 3.1, the most conservative bound for such a neutralino-pair production cross section was set by the OPAL result. The upper bound of the cross section varies according to mass values of the neutralinos. It becomes as much as 70 fb in the parameter space of our interest, $m_{\tilde{\chi}_1^0} \gtrsim m_h/2 \sim 63$ GeV and $120 \lesssim m_{\tilde{\chi}_2^0} \lesssim 140$ GeV.

The numerical results for the GUT and TeV mirage relations of gaugino masses are shown in Figs. 2 and 3, respectively. In the case of the GUT relation, light EW gauginos are mixed with the singlino, and the lightest neutralino becomes lighter. Moreover, the next-to-lightest neutralino also becomes lighter due to the Higgsino-gaugino mixing, which increases the $\tilde{\chi}_1^0\tilde{\chi}_2^0$ production in the LEP II experiment. Hence, only small region of the parameter space, $\tan\beta \lesssim 1.2$ and $120 \text{ GeV} \lesssim \mu_{\text{eff}} \lesssim 130 \text{ GeV}$, is allowed. On the other hand, in the case of the TeV mirage, the EW gauginos are heavy so that the lightest and the next-to-lightest neutralinos are mostly composed of the singlino and the Higgsino. Consequently, the masses of the lightest two neutralinos are heavier than those of the GUT relation case, and thereby avoiding the LEP II constraint for the $\tilde{\chi}_1^0\tilde{\chi}_2^0$ production for broader parameter region, $\tan\beta \lesssim 1.5$ and $130 \text{ GeV} \lesssim \mu_{\text{eff}} \lesssim 170 \text{ GeV}$.

This small $\tan\beta$ scenario has excellent features in the naturalness point of view. The large loop corrections by the stops are not necessary to raise the Higgs boson mass up to 125 GeV as the tree-level Higgs boson mass can be raised enough by the λ -proportional contribution by virtue of the small $\tan\beta$. This ameliorates the fine-tuning problem from the stop sector. Moreover, all massive soft parameters related to the EW symmetry breaking are of order of 100 GeV. When $\tan\beta = 1.3$ and $\mu_{\text{eff}} = 135$ GeV in Fig. 3, for example, the masses related to the EW symmetry breaking are given by

$$m_{H_u} \sim m_{H_d} \sim 200 \text{ GeV}, \quad m_S \sim 600 \text{ GeV}, \quad m_{\tilde{t}} \sim 500 \text{ GeV}. \quad (57)$$

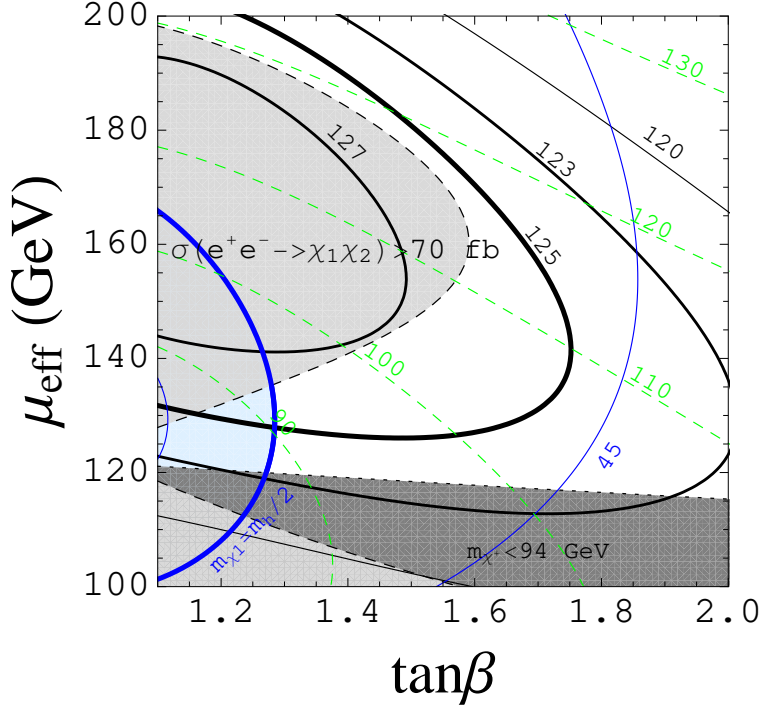


Figure 2: Plot for small $\tan\beta$. Here we set $6M_1 = 3M_2 = M_3 = 1$ TeV, $m_A = 350$ GeV, $m_{\tilde{Q}_3} = m_{\tilde{t}_c} = 500$ GeV, $A_t = 0$, and $\xi_S = -7 \times 10^7$ GeV³. Black curves denote Higgs mass in GeV, blue curves denote $m_{\tilde{\chi}_1^0}$ in GeV, and green dashed curves denote $m_{\tilde{\chi}_2^0}$. The gray-shaded region is excluded by the OPAL [17].

Therefore, the EW symmetry breaking condition can be satisfied up to 5% parameter tuning.

Concerning the cosmology in this scenario, if the LSP is the lightest neutralino, the substantial Higgsino mixing in the LSP becomes the cause of the similar cosmological features as the Higgsino dark matter of the MSSM. Still, due to the large Higgsino-singlino-Higgs coupling from the $\lambda SH_u H_d$ term in the superpotential, the direct detection cross section can be rather large. On the other hand, it is expected that the amount of missing energy in the LHC experiment will not be much different from that of the MSSM since the $m_{\tilde{\chi}_1^0}$ is slightly larger than $m_h/2$. The existence of the light third-generation squarks will lead to the top or bottom-rich signal. The dark matter and the collider signatures at the LHC for the small $\tan\beta$ region will be discussed in more detail in Secs. 4 and 5, respectively.

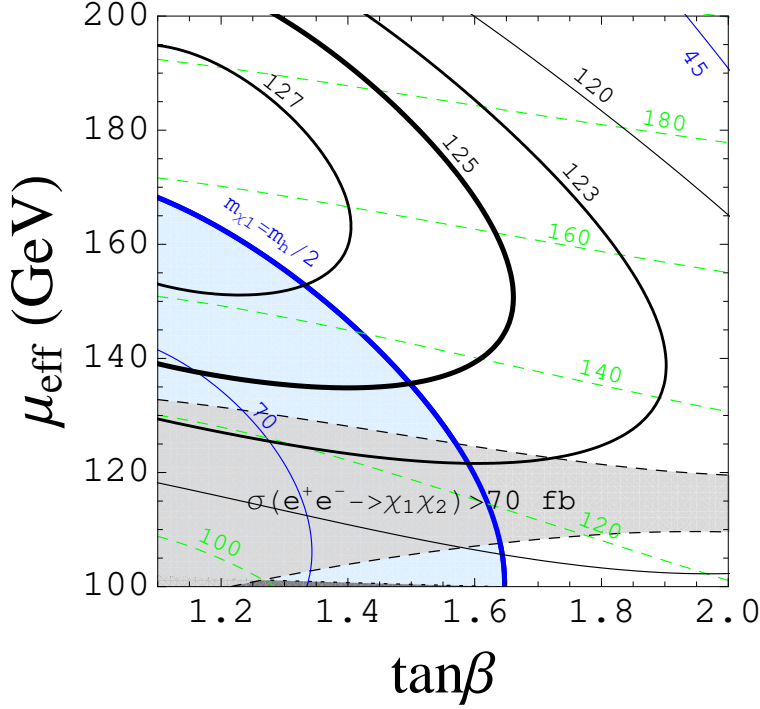


Figure 3: Plot for small $\tan\beta$. Here we set $M_1 = M_2 = M_3 = 1$ TeV, $m_A = 350$ GeV, $m_{\tilde{Q}_3} = m_{\tilde{t}_c} = 500$ GeV, $A_t = 0$, and $\xi_S = -7 \times 10^7$ GeV³. Black curves denote Higgs mass in GeV, blue curves denote $m_{\tilde{\chi}_1^0}$ in GeV, and green dashed curves denote $m_{\tilde{\chi}_2^0}$. The gray-shaded region is excluded by the OPAL [17].

3.3.2 Large $\tan\beta$: very light neutralino scenario

For large values of $\tan\beta \gtrsim 1.6$, the lightest neutralino mass becomes smaller than $m_h/2$, and the Higgs invisible decay mode to a lightest neutralino pair is open. In this region, it is necessary to examine conditions for suppressing the Higgs invisible decay. As argued in (56), it is plausible to put the Higgs mixing parameter c as small as possible in order to make the Higgs invisible decay rate vanishing, while keeping relatively small $\tan\beta$ by which the quartic coupling λ can substantially raise the tree-level Higgs boson mass. As an extreme example, we consider vanishing Higgs mixing parameter c . To achieve this for relatively small $\tan\beta$, we set $\mathcal{M}_{S,12}^2 = 0$ implying

$$(2\lambda^2 v^2 - m_A^2 - m_Z^2) \cos\beta \sin\beta = 0, \quad (58)$$

that is,

$$m_A^2 = 2\lambda^2 v^2 - m_Z^2 \approx (146 \text{ GeV})^2. \quad (59)$$

In this case, the lightest Higgs boson is mostly the up-type, H_u , for $\tan\beta \gtrsim 2$. Here, m_A^2 is not the physical CP-odd Higgs boson mass, but a model parameter defined as $m_A^2 \equiv$

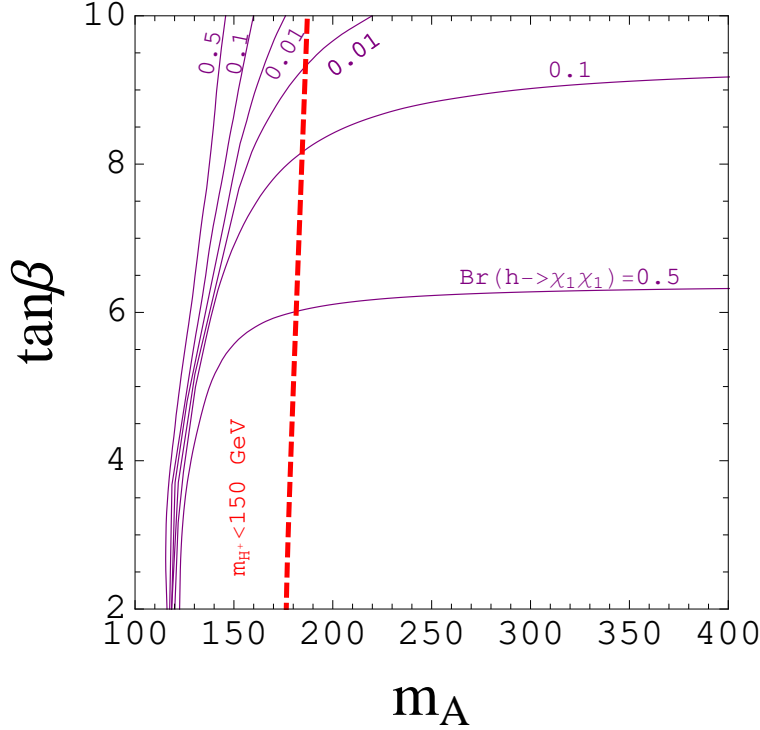


Figure 4: Contours of the branching fraction of the Higgs invisible decay for μ_{eff} and the GUT relation of gaugino masses. In the left side of red dashed region, charged Higgs mass is smaller than 150 GeV so that $\tan \beta \lesssim 4$ is excluded by the charged Higgs search experiment.

$2b_{\text{eff}}/\sin 2\beta$, which indeed corresponds to the CP-odd Higgs boson mass in the MSSM limit. Now, by putting $c = 0$ in (56), one can find

$$\frac{1}{\tan \beta} \simeq \frac{3m_W^2}{M_2\mu_{\text{eff}}} \left(1 + \frac{3\sqrt{2}\lambda^2 v^2}{\mu_{\text{eff}}^2} \right), \quad (60)$$

and thus $\tan \beta \approx 3$ for $\mu_{\text{eff}} = M_2 = 300$ GeV. Although one can suppress the Higgs invisible decay with $\tan \beta \approx 3$ in this way, the small m_A^2 in (59) can lead to the light charged Higgs boson. At tree level, the charged Higgs boson mass is given by

$$m_{H^\pm}^2 = \frac{2(\mu_{\text{eff}}B_{\text{eff}} + \hat{m}_3^2)}{\sin 2\beta} + v^2 \left(\frac{g_2^2}{2} - \lambda^2 \right) = m_A^2 + m_W^2 - \lambda^2 v^2, \quad (61)$$

leading to $m_{H^\pm} \approx 113$ GeV for the parameter choice (59). Such a light charged Higgs boson is excluded by the recent ATLAS search in the decays of top quarks [18]. More generally, the charged Higgs boson mass smaller than 150 GeV and $\tan \beta \lesssim 4$ has been excluded under the assumption of $\text{Br}(H^+ \rightarrow \tau^+ \nu) = 1$. Fig. 4 shows the result of our calculation of the Higgs invisible decay ratio depending on m_A and $\tan \beta$ and the current LHC limit. It should be mentioned that m_A in the horizontal axis is the input parameter at stop mass

scale, so it is different from m_A in (58) that is the value at the weak scale. In addition, since the result includes loop corrections, it is slightly different from what is expected from the tree-level estimation. In Fig. 4, one can find the region of $\tan\beta \gtrsim 4$ and $m_A \sim 130$ GeV in which the Higgs invisible decay ratio becomes vanishingly small. In this region, however, the production cross section and the decay branching fraction of the lightest Higgs boson become different from the SM-like one because of the CP-even Higgs mixing from the mass matrix (33). In order to assess the viability of such non-SM-like Higgs scenario, we would need more complicated study for whole SUSY parameters and collider signatures. We will leave this for future work and focus on the SM-like Higgs phenomenology from now on.

In the case of larger m_A , the invisible decay branching fraction of the Higgs boson drastically increases so that larger $\tan\beta$ is needed for the Higgs invisible decay to vanish as was showed in (56). For $m_A \gtrsim 200$ GeV, the invisible branching fraction becomes nearly independent of m_A since such region corresponds to the MSSM decoupling limit, in which the lightest CP-even Higgs boson becomes SM-like, so we find $c \simeq -\tan\alpha \simeq \cot\beta$. In other words, the Higgs coupling to a neutralino pair (55) depends only on $\tan\beta$. In this region, we need $\tan\beta \gtrsim 9$ for $\text{Br}(h \rightarrow \tilde{\chi}_1^0 \tilde{\chi}_1^0) < 0.1$. It should be noted that this result is obtained with the GUT relation of gaugino masses, and if one considers the TeV mirage relation, the corresponding $\tan\beta$ value becomes larger. For such large $\tan\beta$, the NMSSM feature of the sizable λ contribution to the tree-level Higgs boson mass is lost since $\lambda^2 v^2 \sin^2 2\beta$ in (34) is already small compared to the Z boson contribution $m_Z^2 \cos^2 2\beta$. Thus, it is required to have large loop corrections from the stop sector as in the MSSM.

For the comparison between cases of the GUT and TeV mirage scenarios, we show the Higgs couplings to a neutralino pair and corresponding branching fractions for both cases in Figs. 5 and 6. In the case of the GUT relation, the EW gauginos are light ($M_1 = 160$ GeV and $M_2 = 330$ GeV), so the coupling vanishes when $\tan\beta \sim 12$ as can be seen in Fig. 5(a). This is consistent with the relation (56). Therefore, the branching fraction of the Higgs invisible decay is very small near $\tan\beta \sim 12$ as shown in Fig. 5(b). On the other hand, in the case of TeV mirage relation, the gauginos are relatively heavy ($M_1 = M_2 = 1$ TeV), thus (56) can be satisfied only for very large values of $\tan\beta$. In Fig. 6(a), one can see the solution of (56) at $\tan\beta \sim 42$. Instead, the size of the Higgs coupling to a neutralino pair becomes smaller as $\tan\beta$ becomes larger. Hence, nearly vanishing Higgs invisible decay can be attained when $\tan\beta \gtrsim 20$ as shown in Fig. 6(b).

So far, we have seen that rather large $\tan\beta$ ($9 \lesssim \tan\beta \lesssim 18$ for the GUT and $\tan\beta \gtrsim 20$ for the TeV mirage relation) is needed to reduce the Higgs invisible decay branching fraction below 10% level. Even if we allow the branching fraction up to 50% level, one needs $\tan\beta \gtrsim 6$ for the GUT and $\tan\beta \gtrsim 10$ for the TeV mirage relation. This suppresses the NMSSM contribution to the tree-level Higgs boson mass and there is no difference from the MSSM in the naturalness point of view. However, an important difference arises due to the existence of the very light neutralino. As one can see in (41), the

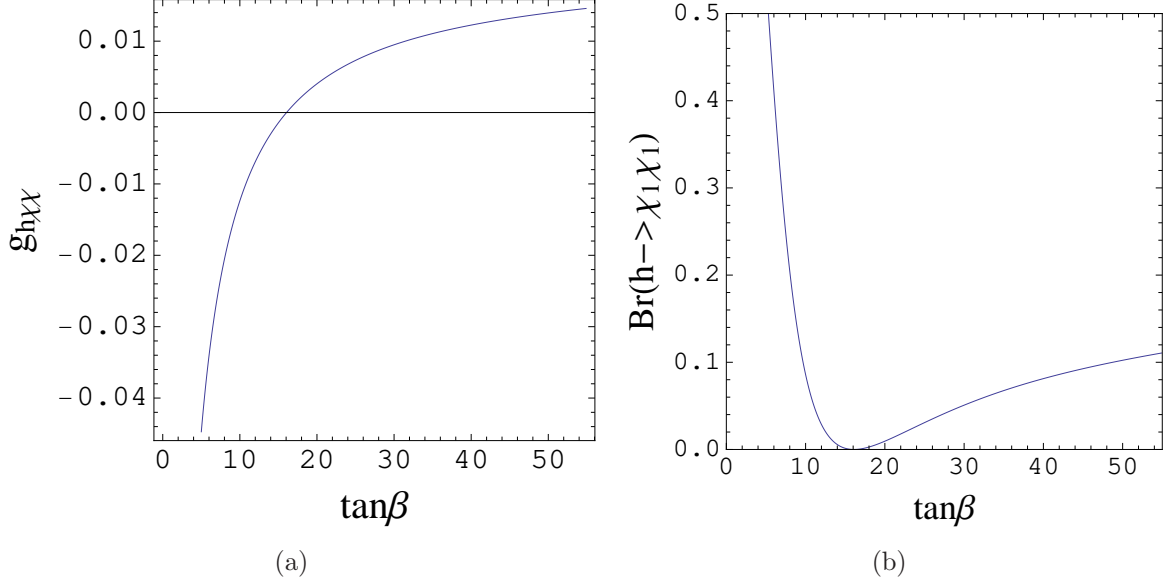


Figure 5: (a) The lightest Higgs coupling to the lightest neutralino pair, (b) Branching fraction of the Higgs invisible decay. In these plots, we use $m_A = 500$ GeV, $\mu_{\text{eff}} = 400$ GeV and the GUT relation of gaugino masses.

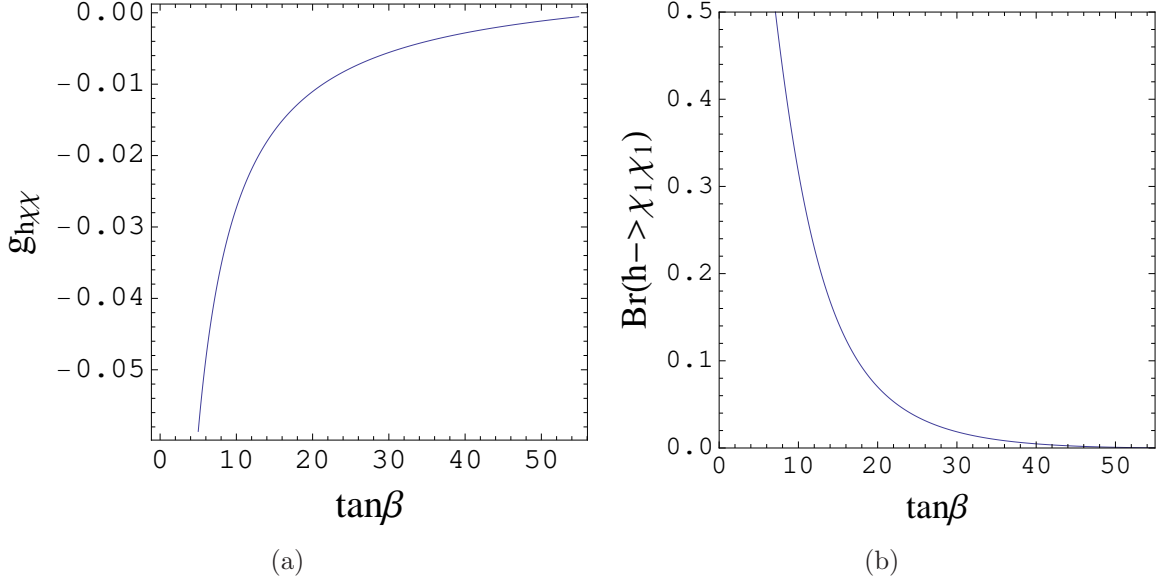


Figure 6: (a) The lightest Higgs coupling to the lightest neutralino pair, (b) Branching fraction of Higgs invisible decay. In these plots, we use $m_A = 500$ GeV, $\mu_{\text{eff}} = 400$ GeV and TeV mirage relation of gaugino masses.

lightest neutralino mass is generally smaller than 15 GeV for $\tan \beta \gtrsim 5$ leading to non-trivial

implications in cosmology and collider signatures. If such a light singlino-like neutralino is the LSP, its annihilation cross section is very small, and thereby overproducing the dark matter density. To avoid this problem, we need a non-standard cosmological history, which will be discussed in Sec. 4. On the other hand, the singlino-like LSP modifies the decay topology of the supersymmetric particles. This will be discussed in Sec. 5.

4 Dark Matter

Let us now discuss the dark matter cosmology of the singlino-like LSP for two regions of small and large $\tan\beta$ that survived the various constraints from particle phenomenology. For each region, the standard LSP dark matter obtained by thermal freeze-out has a difficulty in satisfying the cosmological density and/or the direct detection bound. Instead, the non-standard cosmology driven by the axion supermultiplet, the PQ sector, can provide a viable range of the parameter space. In the following discussions, we assume that R-parity is conserved and the lightest neutralino, mostly singlino, is the LSP disregarding a possibility of lighter axino or gravitino being the LSP.

4.1 Small $\tan\beta$ region ($1 \lesssim \tan\beta \lesssim 2$)

In the small $\tan\beta$ region, the LSP mass $m_{\tilde{\chi}_1^0}$ is around 50 – 70 GeV. As studied in the context of the nMSSM [19], both s -channel Z boson exchange ($\tilde{\chi}_1^0\tilde{\chi}_1^0 \rightarrow Z \rightarrow f\bar{f}$) and s -channel Higgs boson exchange ($\tilde{\chi}_1^0\tilde{\chi}_1^0 \rightarrow h \rightarrow f\bar{f}$) are equally important for the neutralino annihilation cross-section. The effect of the Higgs exchange is more important than in the case of the MSSM since the $h\text{-}\tilde{\chi}_1^0\text{-}\tilde{\chi}_1^0$ coupling (66) is enhanced compared to that of the MSSM. The resulting relic abundance $\Omega_{\tilde{\chi}_1^0}^{\text{TH}}h^2$ is represented in the left panels of Figs. 7 and 8 for the GUT scale unified gaugino masses and the TeV scale mirage mediation, respectively. The superscript “TH” implies the dark matter density produced from thermal freeze-out. In each figure, the narrow contour lines of $\Omega_{\tilde{\chi}_1^0}^{\text{TH}}h^2$ around $10^{-2} - 10^{-4}$ for smaller $\tan\beta$ correspond to the Higgs resonance region, $m_{\tilde{\chi}_1^0} \approx m_h/2$. As $\tan\beta$ increases on the right-hand side of the Higgs resonance, $m_{\tilde{\chi}_1^0} < m_h/2$, $m_{\tilde{\chi}_1^0}$ approaches $m_Z/2$ and thus $\Omega_{\tilde{\chi}_1^0}^{\text{TH}}h^2$ decreases again due to the Z resonance. As $\tan\beta$ decreases on the left-hand side of the Higgs resonance, $m_{\tilde{\chi}_1^0} > m_h/2$, the neutralino relic abundance increases and can reach the correct amount of the dark matter, $\Omega_{\tilde{\chi}_1^0}^{\text{TH}}h^2 \approx 0.11$.

Right panels of Figs. 7 and 8 represent the effective spin-independent elastic scattering cross-section between the nucleon and the dark matter in units of 10^{-9} pb. For the direct detection bound on the scattering cross-section [8], the standard local dark matter density is assumed, that is, $n_X = \rho_{\text{DM}}^{\text{loc}}/m_{\tilde{\chi}_1^0} \simeq 0.3 \text{ cm}^{-3}(\text{GeV}/m_{\tilde{\chi}_1^0})$ corresponding to $\Omega_{\text{DM}}h^2 \approx 0.11$. However, in our parameter region where the thermal relic abundance of the neutralino dark

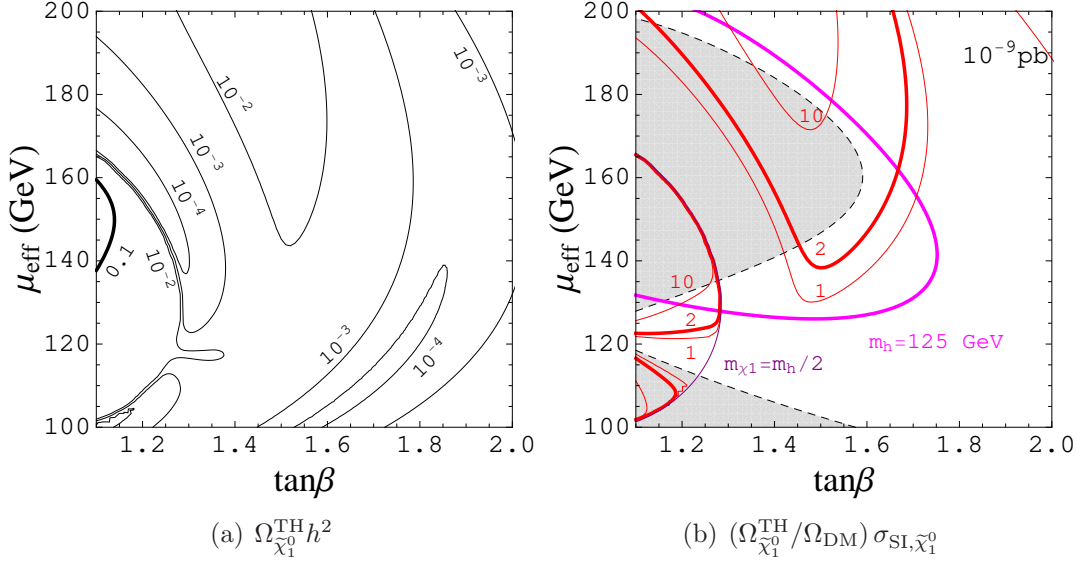


Figure 7: Plot for low $\tan\beta$ with $6M_1 = 3M_2 = M_3 = 1$ TeV. Other parameters are the same as those of Fig. 2. (a) Black curves denote the thermal relic density of the neutralino LSP, $\Omega_{\tilde{\chi}_1^0}^{\text{TH}} h^2$. (b) Red curves denote the central values of the nucleonic scattering cross-section of the lightest neutralino, $(\Omega_{\tilde{\chi}_1^0}^{\text{TH}}/\Omega_{\text{DM}})\sigma_{\text{SI},\tilde{\chi}_1^0}$ in the unit of 10^{-9} pb. The magenta curve denotes 125 GeV Higgs mass, the purple curve denotes $m_{\tilde{\chi}_1^0} = m_h/2$, and the gray-shaded region is excluded by OPAL. For $50 \text{ GeV} \lesssim m_{\tilde{\chi}_1^0} \lesssim 70 \text{ GeV}$, the XENON100 rules out the region $(\Omega_{\tilde{\chi}_1^0}^{\text{TH}}/\Omega_{\text{DM}})\sigma_{\text{SI},\tilde{\chi}_1^0} > 2 \times 10^{-9}$ pb at 90% C.L. [8].

matter is smaller than $\Omega_{\text{DM}} h^2 \simeq 0.11$, the neutralino number density around the Earth decreases by the factor of $\Omega_{\tilde{\chi}_1^0}^{\text{TH}}/\Omega_{\text{DM}}$. Thus, we show the effective cross-section between the nucleon and the assumed dark matter, $(\Omega_{\tilde{\chi}_1^0}^{\text{TH}}/\Omega_{\text{DM}}) \times \sigma_{\text{SI},\tilde{\chi}_1^0}$, where the spin-independent elastic scattering cross-section between the nucleon and the neutralino $\sigma_{\text{SI},\tilde{\chi}_1^0}$ is given by

$$\sigma_{\text{SI},\tilde{\chi}_1^0} = \frac{4}{\pi} \left(\frac{m_{\tilde{\chi}_1^0} m_N}{m_N + m_{\tilde{\chi}_1^0}} \right)^2 f_N^2. \quad (62)$$

Here, N represents the nucleon (p, n) and the constant f_N is

$$\frac{f_N}{m_N} = \sum_{q=u,d,s} f_{Tq}^{(N)} \left(\frac{\alpha_q}{m_q} \right) + \frac{2}{27} \sum_{q=c,b,t} f_{Tq}^{(N)} \left(\frac{\alpha_q}{m_q} \right), \quad (63)$$

where m_q denotes the quark mass, α_q is the coupling constant of the quark level effective Lagrangian term $\mathcal{L}_{\text{eff}} = \alpha_q \tilde{\chi}_1^0 \tilde{\chi}_1^0 \bar{q} q$, and the hadronic matrix elements are given by $m_N f_{Tq}^{(N)} = \langle N | m_q \bar{q} q | N \rangle$ and $f_{Tg}^{(N)} = 1 - \sum_{q=u,d,s} f_{Tq}^{(N)}$ [20]. The numerical values of the matrix element

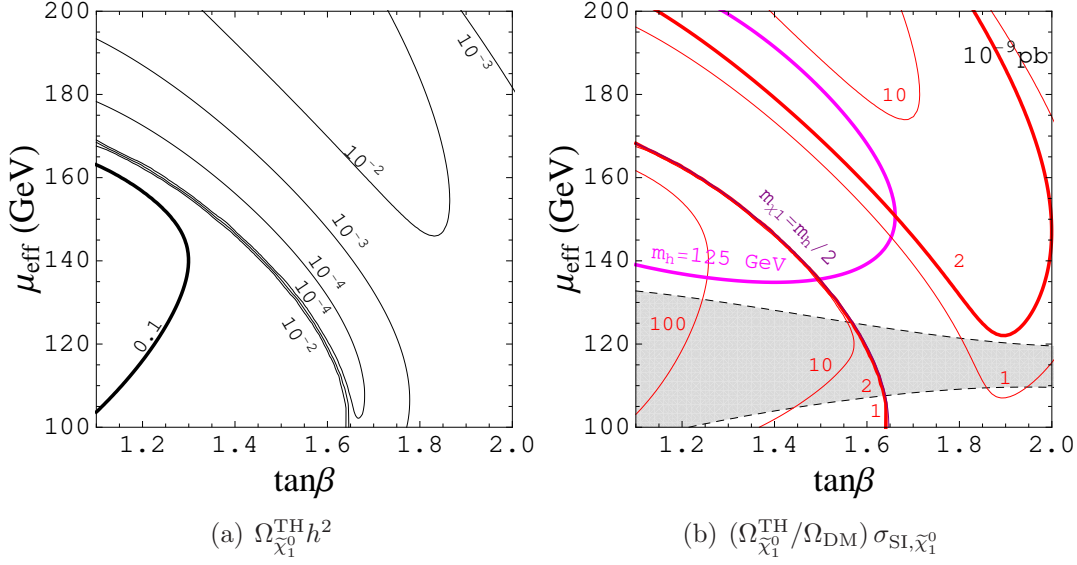


Figure 8: Plot for low $\tan\beta$ with $M_1 = M_2 = M_3 = 1$ TeV. Other parameters are the same as those of Fig. 2. (a) Black curves denote the relic amount of the neutralino LSP, $\Omega_{\tilde{\chi}_1^0}^{\text{TH}} h^2$. (b) Red curves denote the central values of the nucleonic scattering cross-section of the lightest neutralino, $(\Omega_{\tilde{\chi}_1^0}^{\text{TH}}/\Omega_{\text{DM}})\sigma_{\text{SI},\tilde{\chi}_1^0}$ in the unit of 10^{-9} pb. The magenta curve denotes 125 GeV Higgs mass, the purple curve denotes $m_{\tilde{\chi}_1^0} = m_h/2$, and the gray-shaded region is excluded by OPAL. For $50 \text{ GeV} \lesssim m_{\tilde{\chi}_1^0} \lesssim 70 \text{ GeV}$, the XENON100 rules out the region $(\Omega_{\tilde{\chi}_1^0}^{\text{TH}}/\Omega_{\text{DM}})\sigma_{\text{SI},\tilde{\chi}_1^0} > 2 \times 10^{-9}$ pb at 90% C.L. [8].

f_{Tq}^N are determined in [21]

$$\begin{aligned} f_{Tu}^{(p)} &= 0.020 \pm 0.004, & f_{Td}^{(p)} &= 0.026 \pm 0.005, & f_{Ts}^{(p)} &= 0.118 \pm 0.062, \\ f_{Tu}^{(n)} &= 0.014 \pm 0.003, & f_{Td}^{(n)} &= 0.036 \pm 0.008, & f_{Ts}^{(n)} &= 0.118 \pm 0.062. \end{aligned} \quad (64)$$

In our case, the coupling constant α_q is dominantly given by t -channel Higgs exchange diagram,

$$\alpha_q \simeq -\frac{g_{h\tilde{\chi}_1^0\tilde{\chi}_1^0}}{m_h^2} \left(\frac{g_2 m_q S_{11}}{m_W \sin\beta} \right) \quad (65)$$

for the up-type quarks. For the down-type quark, α_q is obtained by the appropriate replacements ($S_{11} \rightarrow S_{21}$, $\sin\beta \rightarrow \cos\beta$). The Higgs-LSP-LSP coupling $g_{h\tilde{\chi}_1^0\tilde{\chi}_1^0}$ is given by

$$\begin{aligned} g_{h\tilde{\chi}_1^0\tilde{\chi}_1^0} &= -g_2 (N_{12} - \tan\theta_W N_{11}) (S_{11} N_{13} - S_{12} N_{14}) \\ &\quad + \sqrt{2}\lambda (S_{13} N_{13} N_{14} + N_{15} (S_{12} N_{13} + S_{11} N_{14})). \end{aligned} \quad (66)$$

The first line in (66) is the same as in the MSSM, and the second line comes from the superpotential term, $\lambda S H_u H_d$. Due to the sizable Higgsino component of the LSP, the

second term dominates $g_{h\tilde{\chi}_1^0\tilde{\chi}_1^0}$. The recent XENON100 data puts an upper limit on the effective spin-independent LSP-nucleon cross-section around 2×10^{-9} pb for the mass range of 50–70 GeV at 90% C.L. [8]. Note that the region that gives $\Omega_{\tilde{\chi}_1^0}^{\text{TH}} h^2 = 0.11$ is far above the XENON100 bound. However, for the points on the 125 GeV Higgs line close to the Higgs resonance point, the XENON100 bound can be avoided because the neutralino thermal relic density can be much below the observed dark matter density. More specifically, we find that the mass difference between $m_{\tilde{\chi}_1^0}$ and $m_h/2$ should be smaller than $\mathcal{O}(0.1)$ GeV,

$$m_{\tilde{\chi}_1^0} - \frac{m_h}{2} \lesssim 0.1 \text{ GeV}. \quad (67)$$

Recall that, since the neutralino contribution to the dark matter density is small, the major component of the dark matter density can come from the axion for $v_{\text{PQ}} \sim 10^{12}$ GeV in our scenario,

$$\Omega_a h^2 \simeq 0.23 \left(\frac{v_{\text{PQ}}}{10^{12} \text{ GeV}} \right)^{7/6} \langle \theta^2 \rangle, \quad (68)$$

where θ is the initial misalignment angle, typically of order one.

Let us note that the PQ-NMSSM has a late-time decaying saxion field s , a CP-even partner of the axion a , which can dilute away the LSP relic density calculated previously. If the PQ sector is stabilized by SUSY breaking effects as discussed in Sec. 2.1, the saxion typically gets a mass of the order of the weak scale, and its interaction with other particles are suppressed by $1/v_{\text{PQ}}$, so it has a long lifetime. It is natural to have a period in the early universe during which the energy density of the universe is dominated by the coherent oscillation of s or vacuum energy of the PQ sector field. At the end of this period ($t \sim 1/\Gamma_s$ where Γ_s is the total decay rate of s), the saxion will decay to produce radiation reheating the Universe at the temperature T_{RH} obtained from the relation $\rho_s(T_{\text{RH}}) \simeq \rho_r(T_{\text{RH}})$. The reheat temperature T_{RH} is given by

$$T_{\text{RH}} \simeq 200 \text{ MeV} \left(\frac{10}{g_*(T_f)} \right)^{1/4} \left(\frac{0.1}{\text{Br}_a} \right)^{1/2} \left(\frac{m_s}{100 \text{ GeV}} \right)^{3/2} \left(\frac{10^{12} \text{ GeV}}{v_{\text{PQ}}} \right), \quad (69)$$

where Br_a is the branching fraction of the saxion decay into the axion pair having the rate $\Gamma_{s \rightarrow aa} = m_s^3/(64\pi v_{\text{PQ}}^2) = \text{Br}_a^{-1} \Gamma_s$ [22]. For $v_{\text{PQ}} = 10^{12}$ GeV, the reheat temperature is much smaller than the freeze-out temperature of the LSP ($T_{\text{RH}} \ll T_f \simeq m_{\tilde{\chi}_1^0}/22 \sim 3$ GeV), and thus the depleted thermal LSP population cannot be regenerated. Furthermore, the non-thermal production of the LSP from the saxion decay can also be forbidden if the saxion mass m_s is taken to be smaller than $2m_{\tilde{\chi}_1^0}$. Therefore, the stringent constraint (67) on the LSP mass can be relaxed.

4.2 Large $\tan \beta$ region ($5 \lesssim \tan \beta$)

In the large $\tan \beta$ region, we found that the lightest neutralino mass is below $\mathcal{O}(5 \text{ GeV})$ from the consideration of the Higgs invisible decay. Since $m_{\tilde{\chi}_1^0}$ is far from the Higgs resonance

region, the LSPs are annihilated into the SM fermion pairs dominantly by the s -channel Z boson exchange, $\tilde{\chi}_1^0 \tilde{\chi}_1^0 \rightarrow Z \rightarrow f \bar{f}$. In the mass range of $1 \text{ GeV} \lesssim m_{\tilde{\chi}_1^0} \lesssim 5 \text{ GeV}$, the LSP relic abundance is given by

$$\begin{aligned} \Omega_{\tilde{\chi}_1^0}^{\text{TH}} h^2 &= 1.07 \times 10^9 \left(\frac{m_{\tilde{\chi}_1^0}}{\sqrt{8\pi} M_{\text{Pl}}} \right) \left(\int_0^{T_f} dT g_*(T)^{1/2} \langle \sigma_{\text{ann}} v \rangle_T \text{ GeV}^2 \right)^{-1} \\ &= 10^3 \gamma_{f\tilde{\chi}_1^0} \left(\frac{x_f}{9} \right)^2 \left(\frac{10}{g_*(T_f)} \right)^{1/2} \left(1 - \frac{4m_{\tilde{\chi}_1^0}^2}{m_Z^2} \right)^2 \left(\frac{2 \text{ GeV}}{m_{\tilde{\chi}_1^0}} \right)^2 \left(\frac{0.04}{|N_{13}^2 - N_{14}^2|} \right)^2, \end{aligned} \quad (70)$$

where T_f is the freeze-out temperature of $\tilde{\chi}_1^0$, $x_f = m_{\tilde{\chi}_1^0}/T_f$ is around $8 \sim 10$ (15) for $m_{\tilde{\chi}_1^0} \sim 1 \text{ GeV}$ (5 GeV), and $g_*(T_f) \simeq 10$ for $T_f \sim 100 \text{ MeV}$. The order-one constant $\gamma_{f\tilde{\chi}_1^0}$ basically counts the number of fermions lighter than the LSP. The neutralino mixing elements (52) and (53) give

$$|N_{13}^2 - N_{14}^2| \simeq \frac{\lambda^2 v^2 \sin^2 \beta}{\mu_{\text{eff}}^2} \simeq 0.04 \left(\frac{m_{\tilde{\chi}_1^0}}{2 \text{ GeV}} \right) \left(\frac{\tan \beta}{20} \right) \left(\frac{500 \text{ GeV}}{\mu_{\text{eff}}} \right) \quad (71)$$

for large $\tan \beta$. Recall that $|N_{13}^2 - N_{14}^2|$ is bounded by 0.13 as in (46). Therefore, in order to avoid the overclosure dark matter density, the neutralino abundance has to be depleted by the factor of $\Delta \sim 10^4 - 10^2$ for $m_{\tilde{\chi}_1^0} \sim 1 - 5 \text{ GeV}$.

In the large $\tan \beta$ region, $m_{\tilde{\chi}_1^0}$ is sensitive to λ while the Higgs mass is not, and can be much smaller than 1 GeV if we allow for λ smaller than the nominal choice 0.7. For instance, one finds $m_{\tilde{\chi}_1^0} \sim 10 \text{ MeV}$ for $\lambda \sim 0.1$. In this case, the freeze out temperature T_f is larger than $m_{\tilde{\chi}_1^0}$ and becomes a few GeV. The relic abundance is then given by

$$\Omega_{\tilde{\chi}_1^0}^{\text{TH}} h^2 \simeq 0.3 \times 10^5 \left(\frac{m_{\tilde{\chi}_1^0}}{30 \text{ MeV}} \right) \left(\frac{100}{g_*(T_f)} \right). \quad (72)$$

Thus, even larger dilution factor $\Delta \sim 10^5$ is needed for $m_{\tilde{\chi}_1^0} = \mathcal{O}(10 \text{ MeV})$.

It is amusing to note that the dilution mechanism by the saxion field discussed in the previous subsection can successfully deplete the LSP thermal abundance as well as produce the right amount of the non-thermal LSP relic density. Since the singlino LSP is light enough to be produced by the saxion decay, we need to check how sizable amount of the LSP dark matter can be produced in this process. Such a non-thermal production is controlled by the ratio $m_{\tilde{\chi}_1^0}/m_s$ as the $s\text{-}\tilde{\chi}_1^0\text{-}\tilde{\chi}_1^0$ coupling is proportional to $m_{\tilde{\chi}_1^0}/v_{\text{PQ}}$ whereas the $s\text{-}a\text{-}a$ coupling is proportional to m_s/v_{PQ} . We here consider the case $m_s \sim 100 \text{ GeV}$, then the dominant saxion decay mode can be $s \rightarrow b\bar{b}$ whose coupling is proportional to $c_{sH} m_b \tan \beta / v_{\text{PQ}}$, where c_{sH} is an order-one parameter parameterizing the saxion-Higgs mixing. For $\tan \beta \gtrsim 25$, the $s\text{-}b\text{-}\bar{b}$ coupling can be larger than the $s\text{-}a\text{-}a$ coupling allowing for $\text{Br}_a < 0.1$. Now, one can find the relic abundance of non-thermally produced LSP through the decay $s \rightarrow \tilde{\chi}_1^0 \tilde{\chi}_1^0$ as follows.

$$\Omega_{\tilde{\chi}_1^0}^{\text{NTH}} h^2 = 0.1 \gamma_{s\tilde{\chi}_1^0\tilde{\chi}_1^0} \left(\frac{m_{\tilde{\chi}_1^0}}{30 \text{ MeV}} \right)^3 \left(\frac{100 \text{ GeV}}{m_s} \right) \left(\frac{T_{\text{RH}}}{10 \text{ MeV}} \right), \quad (73)$$

where $\gamma_{s\tilde{\chi}_1^0\tilde{\chi}_1^0}$ is the order-one constant controlling the $s\text{-}\tilde{\chi}_1^0\text{-}\tilde{\chi}_1^0$ coupling. The above relation shows that the light singlino LSP abundance can be in the right range for $m_{\tilde{\chi}_1^0} \sim 30$ MeV (obtainable for, e.g., $\lambda \simeq 0.07$, $\tan \beta = 25$, $\mu_{\text{eff}} = 300$ GeV), $m_s \sim 100$ GeV, and $v_{\text{PQ}} \sim 10^{13}$ GeV. Since we used the PQ symmetry breaking scale v_{PQ} larger than 10^{12} GeV, we also have to consider the axion dark matter abundance. The entropy dumping from the saxion decay at $T_{\text{RH}} = \mathcal{O}(10)$ MeV can dilute the axion relic density as well. In this case, the axion dark matter at low decay temperature is given by [22]

$$\Omega_a h^2 \simeq 3 \times 10^{-3} \left(\sqrt{\frac{g_*(T_{\text{RH}})}{10}} \left(\frac{T_{\text{RH}}}{10 \text{ MeV}} \right)^2 \right)^{0.98} \left(\frac{v_{\text{PQ}}}{10^{13} \text{ GeV}} \right)^{1.5} \left(\frac{200 \text{ MeV}}{\Lambda_{\text{QCD}}} \right)^{1.9} \langle \theta^2 \rangle, \quad (74)$$

which is negligible.

5 Collider signature at the LHC

In this section, we study the collider signature of the PQ-NMSSM through the benchmark parameter points chosen in the previous sections with the TeV scale mirage relation of gaugino masses. The mass spectra and branching ratios of the sparticles and Higgs bosons have been calculated with the modified codes of NMSSMTOOLS, and are given in Tables 2 (4) and 3 (5), respectively, for each benchmark point with a small (large) $\tan \beta$. For the small $\tan \beta$ point, the stop mass can be as light as ~ 500 GeV consistent with the 125 GeV Higgs boson. Whereas in the large $\tan \beta$ region, one needs heavy stops (~ 1 TeV) with a large mixing to enhance the Higgs boson mass.

In the small $\tan \beta$ scenario, the main decay modes are similar to those of the typical MSSM scenario with light stops and sbottoms owing to the large mixing between the singlino and the Higgsino. On the other hand, in the large $\tan \beta$ scenario, the existence of the very light singlino LSP prevents the direct decay of the sparticles into the LSP. In most of the time, it results in the additional decay step comparing to the similar MSSM decay processes. The main decay processes of the benchmark point in the large $\tan \beta$ scenario will be

- $\tilde{g} \rightarrow \tilde{t}_1 t \rightarrow \tilde{\chi}_1^\pm b t \rightarrow \tilde{\chi}_1^0 W b t$,
- $\tilde{g} \rightarrow \tilde{t}_1 t \rightarrow \tilde{\chi}_2^0 t t \rightarrow \tilde{\chi}_1^0 Z (H_1) t t$,
- $\tilde{g} \rightarrow \tilde{b}_1 b \rightarrow \tilde{\chi}_1^\pm t b \rightarrow \tilde{\chi}_1^0 W t b$,
- $\tilde{g} \rightarrow \tilde{b}_1 b \rightarrow \tilde{\chi}_2^0 b b \rightarrow \tilde{\chi}_1^0 Z (H_1) b b$.

Hereafter, the SM-like Higgs boson h will be denoted by H_1 representing the lightest among three CP-even Higgs bosons. Therefore, the final states will be dominantly multi-jet,

Table 2: Sparticle and Higgs masses (in GeV) of the PQ-NMSSM benchmark point in the small $\tan\beta$ scenario.

\tilde{g}	\tilde{u}_L	\tilde{u}_R	\tilde{t}_1	\tilde{t}_2	\tilde{b}_1	\tilde{b}_2	\tilde{e}_L	\tilde{e}_R	$\tilde{\tau}_1$	$\tilde{\tau}_2$		
1119	2033	2033	492	542	504	506	2000	2000	2000	2000		
$\tilde{\chi}_1^0$	$\tilde{\chi}_2^0$	$\tilde{\chi}_3^0$	$\tilde{\chi}_4^0$	$\tilde{\chi}_5^0$	$\tilde{\chi}_1^\pm$	$\tilde{\chi}_2^\pm$	H_1	H_2	H_3	A_1	A_2	H^\pm
63	134	206	992	1030	129	1029	125	347	609	339	618	341

Table 3: Main decay modes in % for the sparticles and the lightest Higgs boson of the PQ-NMSSM benchmark point in the small $\tan\beta$ scenario.

$\tilde{g} \rightarrow \tilde{t}_2 t$	32.0	$\tilde{t}_2 \rightarrow \tilde{\chi}_1^\pm b$	32.8	$\tilde{\chi}_1^\pm \rightarrow \tilde{\chi}_1^0 W^*$	100.0
$\tilde{g} \rightarrow \tilde{t}_1 t$	16.7	$\tilde{t}_2 \rightarrow \tilde{\chi}_2^0 t$	26.1	$\tilde{\chi}_2^0 \rightarrow \tilde{\chi}_1^0 Z^*$	99.8
$\tilde{g} \rightarrow \tilde{b}_2 b$	25.8	$\tilde{t}_2 \rightarrow \tilde{\chi}_1^0 t$	27.6	$H_1 \rightarrow b\bar{b}$	62.9
$\tilde{g} \rightarrow \tilde{b}_1 b$	25.5	$\tilde{t}_1 \rightarrow \tilde{\chi}_1^\pm b$	46.9	$H_1 \rightarrow WW^*$	19.2
		$\tilde{t}_1 \rightarrow \tilde{\chi}_2^0 t$	14.9	$H_1 \rightarrow ZZ^*$	2.1
		$\tilde{t}_1 \rightarrow \tilde{\chi}_1^0 t$	19.0	$H_1 \rightarrow \gamma\gamma$	0.2
		$\tilde{b}_2 \rightarrow \tilde{\chi}_1^\pm t$	99.8		
		$\tilde{b}_1 \rightarrow \tilde{\chi}_1^\pm t$	99.1		

coming from the multi-top/bottom, and $H_1/Z/W$ + missing energy, that may survive the early LHC searches on the channels with (two to four) jets and large missing energy [23].⁴ Furthermore, in this parameter point, the heavier neutralinos will eventually decay into the light singlino LSP, which make the missing energy generically small as claimed recently in [26]. This will reduce the efficiency of the searches on the channels with large jet multiplicities and missing energy [27, 28]. Another notable feature of these points is the relatively light stops and sbottoms, which would make the top and/or bottom-rich signal

⁴ This was also claimed in [24, 25] in the context of \mathbb{Z}_3 -invariant NMSSM. Here, we stress that the relatively light singlino-like LSP can be naturally attained in the PQ-NMSSM.

Table 4: Sparticle and Higgs masses (in GeV) of the PQ-NMSSM benchmark point in the large $\tan\beta$ scenario.

\tilde{g}	\tilde{u}_L	\tilde{u}_R	\tilde{t}_1	\tilde{t}_2	\tilde{b}_1	\tilde{b}_2	\tilde{e}_L	\tilde{e}_R	$\tilde{\tau}_1$	$\tilde{\tau}_2$		
1166	2031	2031	837	1158	1014	1036	1001	1001	995	1007		
$\tilde{\chi}_1^0$	$\tilde{\chi}_2^0$	$\tilde{\chi}_3^0$	$\tilde{\chi}_4^0$	$\tilde{\chi}_5^0$	$\tilde{\chi}_1^\pm$	$\tilde{\chi}_2^\pm$	H_1	H_2	H_3	A_1	A_2	H^\pm
0.03	298	307	987	1023	301	1023	123	683	2510	683	2510	687

Table 5: Main decay modes in % for the sparticles and the lightest Higgs boson of the PQ-NMSSM benchmark point in the small $\tan\beta$ scenario.

$\tilde{g} \rightarrow \tilde{t}_1 t$	75.5	$\tilde{t}_1 \rightarrow \tilde{\chi}_1^\pm b$	37.8	$\tilde{\chi}_1^\pm \rightarrow \tilde{\chi}_1^0 W$	100.0
$\tilde{g} \rightarrow \tilde{b}_2 b$	11.0	$\tilde{t}_1 \rightarrow \tilde{\chi}_2^0 t$	35.5	$\tilde{\chi}_2^0 \rightarrow \tilde{\chi}_1^0 Z$	56.0
$\tilde{g} \rightarrow \tilde{b}_1 b$	13.5	$\tilde{t}_1 \rightarrow \tilde{\chi}_1^0 t$	0.1	$\tilde{\chi}_2^0 \rightarrow \tilde{\chi}_1^0 H_1$	44.0
		$\tilde{b}_2 \rightarrow \tilde{t}_1 W$	17.2	$H_1 \rightarrow b\bar{b}$	67.1
		$\tilde{b}_2 \rightarrow \tilde{\chi}_1^\pm t$	55.6	$H_1 \rightarrow WW^*$	15.9
		$\tilde{b}_2 \rightarrow \tilde{\chi}_2^0 b$	12.2	$H_1 \rightarrow ZZ^*$	1.6
		$\tilde{b}_2 \rightarrow \tilde{\chi}_1^0 b$	$\simeq 0.0$	$H_1 \rightarrow \gamma\gamma$	0.2
		$\tilde{b}_1 \rightarrow \tilde{t}_1 W$	29.0		
		$\tilde{b}_1 \rightarrow \tilde{\chi}_1^\pm t$	60.4		
		$\tilde{b}_1 \rightarrow \tilde{\chi}_2^0 b$	60.4		
		$\tilde{b}_1 \rightarrow \tilde{\chi}_1^0 b$	$\simeq 0.0$		

events. The recent constraints on the stop and sbottom masses were set by the searches on the gluino-mediated production [29] and the direct production of the stops and the sbottoms [30,31]. The search results do not affect our study much as the gluino is chosen to be quite heavy and the squark masses are set above the exclusion bound.

In order to study the collider phenomenology of our scenarios, we have generated

Monte Carlo (MC) event samples for a proton-proton collision at 14 TeV by HERWIG++ 2.5.2 [32]. The generated event samples have been scaled to 10 fb^{-1} integrated luminosity. For the sake of the simple analysis, we consider only the leading-order cross sections calculated with HERWIG++ and the CTEQ6L [33] parton distribution functions (PDF). The generator-level event samples have been further processed with the fast detector simulation program DELPHES 2.0 [34] using the ATLAS detector card. Jets are reconstructed using the anti- k_t jet clustering algorithm [35] with radius parameter of 0.4. Isolated electrons (muons) are required to have the transverse momentum $p_T > 20$ (10) GeV and the pseudo-rapidity $|\eta| < 2.47$ (2.4). In the recent version of DELPHES, the missing transverse momenta \cancel{p}_T are defined as the negative vector sum of the transverse momenta of all the calorimetric cells and muon candidates. On top of that, we resolve overlaps between jets with $|\eta| < 2.8$ and leptons by following the recent ATLAS analysis [27]. Jets lying within a distance $\Delta R \equiv \sqrt{(\Delta\eta)^2 + (\Delta\phi)^2} < 0.2$ of an electron are discarded. Then, any lepton remaining within a distance $\Delta R < 0.4$ of such jet is discarded. Finally, all jets with $|\eta| > 2.8$ are discarded. From now on, we will use only the remaining electrons, muons, and jets for the analysis.

The dominant SM background processes in the study of the signal with large jet multiplicities are the top-pair process and W or Z bosons in association with jets. The di-boson and the single-top processes can contribute to the backgrounds as well, but they are negligible. For the simple study to estimate the background effects, we here consider only the top-pair process. Since our study concerns mainly the signal events with a large number of jets, fully hadronic, semi-leptonic, and fully leptonic $t\bar{t}$ events with up to two additional partons in the matrix element were generated with ALPGEN 2.14 [36] and CTEQ6L PDF sets. The parton showering to generate additional jets, and the fragmentation and hadronization are performed by HERWIG++. The MC samples have been processed with the DELPHES to reconstruct jets and isolated leptons and adjust the detector effects.

To suppress the backgrounds, we impose the basic event selection cuts as follows.

- (i) At least 6 jets with $p_T > 80 \text{ GeV}$,
- (ii) no isolated electron or muon,
- (iii) missing transverse energy $\cancel{E}_T > 80 \text{ GeV}$,
- (iv) $\mathcal{S}_T > 0.2$.

Here, \mathcal{S}_T is the transverse sphericity defined as

$$\mathcal{S}_T \equiv \frac{2\lambda_2}{\lambda_1 + \lambda_2}, \quad (75)$$

where λ_1 and λ_2 are the eigenvalues of the 2×2 sphericity tensor $\mathcal{S}_i^j = \sum_k p_{ki} p^{kj}$ of the reconstructed objects [37]. This variable is known to be useful for suppressing QCD events,

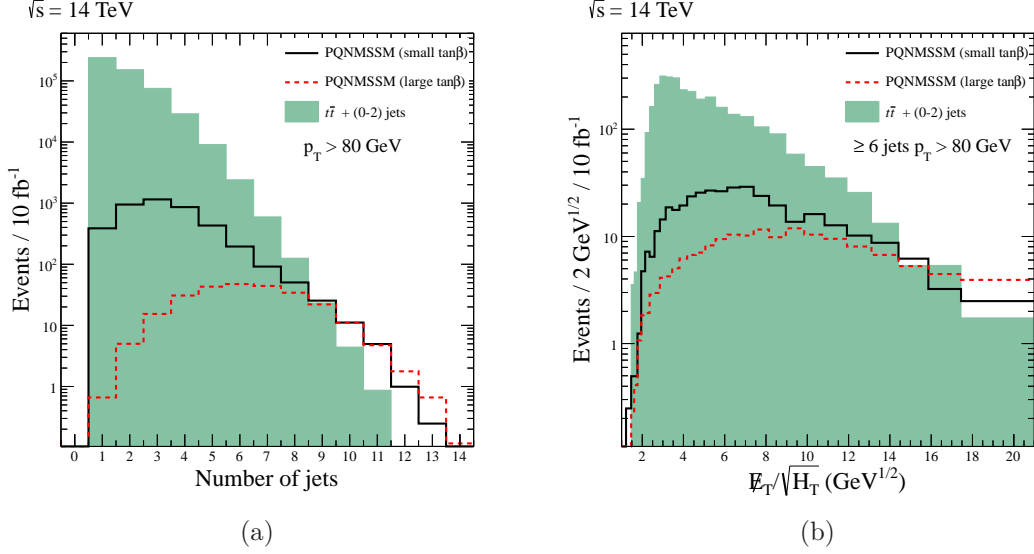


Figure 9: The distributions of (a) the jet multiplicities and (b) the $E_T/\sqrt{H_T}$ for the signal events and $t\bar{t} + \text{jets}$.

in which back-to-back configurations ($\mathcal{S}_T \sim 0$) are dominated. Although such backgrounds are not considered here, this variable will be included in the analysis. In the ATLAS MC study for the inclusive SUSY search [37], the azimuthal angular separation cut, $\Delta\phi(\text{jet} - \not{\mathbf{p}}_T)$, is imposed further to reduce the jet mis-measurement effect. However, it has been recently noted that this cut variable may lose the efficiency if the second-lightest neutralino $\tilde{\chi}_2^0$ was boosted and the lightest Higgs boson H_1 or Z boson decayed into $b\bar{b}$, aligned with the $\not{\mathbf{p}}_T$ vector [25]. We also note that the cut on the missing transverse energy is required to reduce the fully hadronic $t\bar{t}$ background process, even though it should be relatively milder than the typical SUSY searches because of the small missing energy.

We show the jet multiplicity distributions for the signals and backgrounds after applying the basic selection cuts in Fig. 9(a). One can see that there are relatively the more number of energetic jets in the case of the benchmark point with the large $\tan\beta$ scenario. It is mainly due to $t\bar{t}$ or $b\bar{b}$ productions in the small $\tan\beta$ scenario and the additional decay step caused by the existence of the singlino LSP as discussed above. In Fig. 9(b), it is shown the distribution of the ratio $E_T/\sqrt{H_T}$, where H_T is the scalar sum of the transverse momenta of all jets with $p_T > 50$ GeV and $|\eta| < 2.8$. This variable has been known to be useful to increase the performance of the missing energy reconstruction [28]. We require the condition of $E_T/\sqrt{H_T}$ being larger than $4 \text{ GeV}^{1/2}$ in addition to the basic event selection cuts. By employing this cut variable on top of the basic selections cuts, the jet multiplicity distributions are shown in Fig. 10(a). One can see that the background has been reduced, while the signals are remained almost untouched, in the region of the large jet multiplicity.

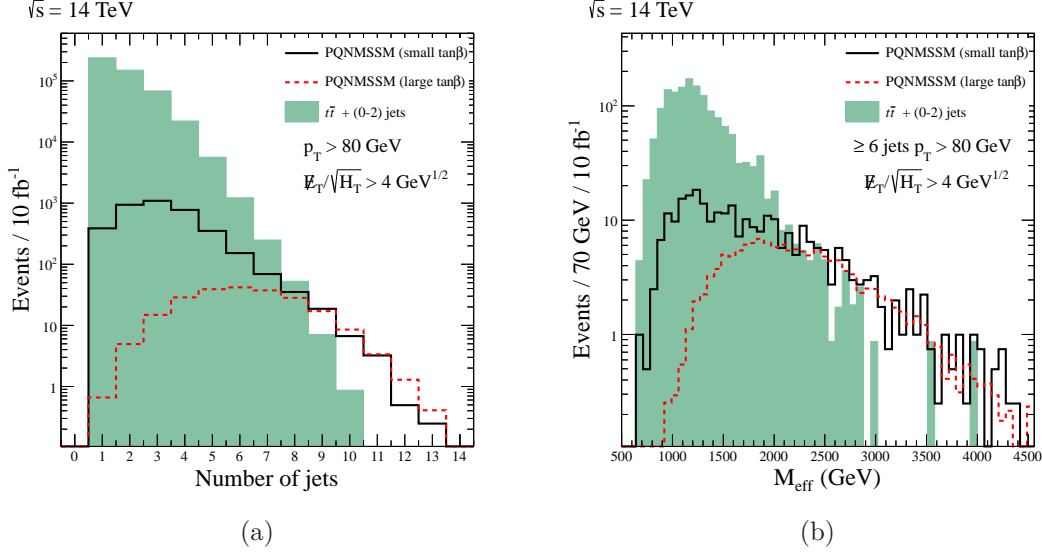


Figure 10: The distributions of (a) the jet multiplicities and (b) the M_{eff} for the signal events and $t\bar{t} + \text{jets}$ with imposing the $\cancel{E}_T/\sqrt{H_T} > 4 \text{ GeV}^{1/2}$ cut.

In Fig. 10(b), we also show the distribution of the effective mass defined as

$$M_{\text{eff}} \equiv \cancel{E}_T + \sum_{\text{jets}} p_T, \quad (76)$$

where the summation is over all jets with $p_T > 50 \text{ GeV}$ and $|\eta| < 2.8$ in the event. The M_{eff} has been known to be a good variable for discriminating SUSY signal events from SM backgrounds [38]. In the literature, it was noted that the peak position of the M_{eff} distribution has a strong correlation with the SUSY mass scale. In the case of the small $\tan\beta$ point, the M_{eff} distribution is peaked in the lower position than that in the case of the large $\tan\beta$ point. This is because of a sizable amount of direct production rates of the light stops and sbottoms, whereas the events of the large $\tan\beta$ point consist practically of the gluino-pair process.

For a crude estimation of the signal significance, we show how the cross sections of the signals and the backgrounds are changing under each event selection cut in Table 6. Although the more accurate estimation should be performed by considering higher-order cross sections, optimizing the cut values by the multivariate analysis techniques, and thorough understanding of the systematic uncertainties, which are beyond the scope our work, one can expect that the 5σ discovery for both PQ-NMSSM scenarios will be possible within several fb^{-1} of the integrated luminosity.

The next issue after the discovery will be the measurement of the masses and spins of the sparticles. This is quite challengeable owing to the several top quarks in the intermedi-

Table 6: Cut flows of the signals and backgrounds in fb.

Selection cuts	PQ-NMSSM		$t\bar{t}$	$t\bar{t} + 1 \text{ jet}$	$t\bar{t} + 2 \text{ jets}$
	small $\tan\beta$	large $\tan\beta$			
$\geq 6 \text{ jets with } p_T > 80 \text{ GeV}$	105.7	57.3	450.2	1650.6	2055.8
Lepton veto	51.8	20.5	359.0	1259.8	1528.9
$\cancel{E}_T > 80 \text{ GeV}$	44.7	19.4	29.7	148.1	219.1
$\mathcal{S}_T > 0.2$	38.0	16.6	23.9	119.6	173.0
$\cancel{E}_T/\sqrt{H_T} > 4 \text{ GeV}^{1/2}$	28.6	13.8	12.7	58.8	82.8
$M_{\text{eff}} > 1000 \text{ GeV}$	26.2	13.8	8.4	45.9	67.4
$M_{\text{eff}} > 1500 \text{ GeV}$	16.6	12.4	1.0	11.5	19.5

ate states. It should be studied the way to resolve the very highly intricate combinatorial uncertainties and increase the efficiency of the top quark reconstruction in this situation.

6 Conclusions

Motivated by the axion solution of the strong CP problem and the recent discovery of a 125 GeV Higgs boson at the LHC, we investigated phenomenological consequences of the PQ symmetry realized in the context of NMSSM. The minimal form of the PQ-NMSSM, in which the singlino mass comes only from the singlino-Higgsino mixing and thus the LSP from the singlino-Higgsino sector becomes lighter than about 70 GeV, is shown to be tightly constrained by the Higgs invisible decay if the LSP is a candidate of the dark matter and its relic density is determined by the standard freeze-out process.

Taking $\lambda = 0.7$, which remains perturbative up to the PQ scale for $\tan\beta$ close to 1, the 125 GeV Higgs can be obtained for stop mass around 500 GeV. Such a small $\tan\beta$ is favored as the Higgs invisible decay can be forbidden kinematically ($m_{\tilde{\chi}_1^0} > m_h/2$). However, it requires a large Higgsino component for the LSP and thus the recent XENON100 bound on the nucleonic cross-section of the LSP at 90% C.L. excludes almost all the parameter region except a narrow band of the LSP mass close to the Higgs resonance point ($m_{\tilde{\chi}_1^0} - m_h/2 < 0.1 \text{ GeV}$) which suppresses the thermal LSP relic density significantly. We also note that a late decay of the saxion inherent in the model can produce a huge amount of entropy diluting away the thermal LSP abundance. Then, the severe constraint on the LSP mass

is invalidated. For larger $\tan\beta$, the LSP mass becomes smaller opening the Higgs invisible decay. In this case, a cancellation can be arranged to suppress the Higgs-LSP-LSP coupling. Combined with the charged Higgs mass bound at the LHC, the Higgs invisible decay branching fraction is shown to become smaller than 10% for $\tan\beta > 9$. In this parameter region, the NMSSM contribution to the Higgs boson mass is negligible and thus a large stop mass ~ 1 TeV is needed to get the Higgs mass of 125 GeV. As the LSP is almost purely singlino for large $\tan\beta$, its thermal freeze-out density is orders of magnitude larger than required. However, it turns out that a late decay of the saxion, washing out the dangerous thermal LSP relics again, can produce the right amount of non-thermal dark matter population for the singlino mass of order 10 MeV with $\lambda \sim 0.1$.

Generic collider signatures of the PQ-NMSSM with a light singlino-like LSP are multi-jets from multi-top/bottom and $h/Z/W$ plus missing energy in the final states. Taking two benchmark points for small and large $\tan\beta$, we analyzed such signals at the 14 TeV LHC to find that a 5σ discovery is possible for a few fb^{-1} of the integrated luminosity.

Let us finally note that the unsatisfactory dark matter properties applied to the minimal PQ-NMSSM in the standard cosmology can be evaded in a more general PQ-NMSSM allowing a suitable bare singlino mass term.

Acknowledgements

KJB, SHI, CBP and CSS gratefully acknowledges the hospitality of KIAS where part of this work was carried out. KJB is supported by TJ Park Postdoctoral Fellowship of POSCO TJ Park Foundation. KC and SHI are supported by the National Research Foundation of Korea(NRF) grant funded by the Korea government(MEST) (No. 2007-0093865 and No. 2012R1A2A2A05003214). KJB, KC and SHI are also supported by the BK21 project by the Korean Government. CBP is partially supported by the grants FPA2010-17747, Consolider-CPAN (CSD2007-00042) from the MICINN, HEPHACOS-S2009/ESP1473 from the C. A. de Madrid and the contract “UNILHC” PITN-GA-2009-237920 of the European Commission. CSS was supported by Basic Science Research Program through the National Research Foundation of Korea (NRF) funded by the Ministry of Education, Science and Technology (No. 2011-0011083). CSS acknowledges the Max Planck Society (MPG), the Korea Ministry of Education, Science and Technology (MEST), Gyeongsangbuk-Do and Pohang City for the support of the Independent Junior Research Group at the Asia Pacific Center for Theoretical Physics (APCTP).

Appendix

A Neutralino mixing matrices

The neutralino mass matrix is given in (40), which can be diagonalized by the method of perturbative diagonalization as in [39],

$$\mathcal{M}^{\text{diag}} = N\mathcal{M}_{\tilde{\chi}^0}N^T = VU\mathcal{M}_{\tilde{\chi}^0}U^TV^T = V\mathcal{M}V^T, \quad (77)$$

where

$$U = \begin{pmatrix} 1 & 0 & 0 & 0 & 0 \\ 0 & 1 & 0 & 0 & 0 \\ 0 & 0 & \frac{1}{\sqrt{2}} & -\frac{1}{\sqrt{2}} & 0 \\ 0 & 0 & \frac{1}{\sqrt{2}} & \frac{1}{\sqrt{2}} & 0 \\ 0 & 0 & 0 & 0 & 1 \end{pmatrix} \quad (78)$$

and

$$\mathcal{M} = \begin{pmatrix} M_1 & 0 & -g_1(v_u + v_d)/2 & g_1(v_u - v_d)/2 & 0 \\ & M_2 & g_2(v_u + v_d)/2 & -g_2(v_u - v_d)/2 & 0 \\ & & \mu_{\text{eff}} & 0 & -\lambda(v_u - v_d)/\sqrt{2} \\ & & & -\mu_{\text{eff}} & -\lambda(v_u + v_d)/\sqrt{2} \\ & & & & 0 \end{pmatrix}. \quad (79)$$

We split the mass matrix into the diagonal part and the off-diagonal part, $\mathcal{M} = \mathcal{M}^D + \mathcal{M}^O$, where $\mathcal{M}^D = \text{diag}(M_1, M_2, \mu_{\text{eff}}, -\mu_{\text{eff}}, 0)$ and \mathcal{M}^O is the rest. In the leading order, we have

$$V_{nm}^{(1)} = \frac{\mathcal{M}_{mn}^O}{\mathcal{M}_{nn}^D - \mathcal{M}_{mm}^D}. \quad (80)$$

In the perturbative limit, we find that

$$V_{51}^{(1)} = -\frac{\mathcal{M}_{15}^O}{M_1} = 0, \quad (81)$$

$$V_{52}^{(1)} = -\frac{\mathcal{M}_{25}^O}{M_2} = 0, \quad (82)$$

$$V_{53}^{(1)} = -\frac{\mathcal{M}_{35}^O}{\mu_{\text{eff}}} = \frac{\lambda v(\sin \beta - \cos \beta)}{\sqrt{2}\mu_{\text{eff}}}, \quad (83)$$

$$V_{54}^{(1)} = \frac{\mathcal{M}_{45}^O}{\mu_{\text{eff}}} = -\frac{\lambda v(\sin \beta + \cos \beta)}{\sqrt{2}\mu_{\text{eff}}}. \quad (84)$$

In the second order,

$$V_{nm}^{(2)} = \sum_{k \neq n} \frac{\mathcal{M}_{mk}^O \mathcal{M}_{nk}^O}{(\mathcal{M}_{nn}^D - \mathcal{M}_{mm}^D)(\mathcal{M}_{nn}^D - \mathcal{M}_{kk}^D)} - \frac{1}{2} \sum_{k \neq n} \frac{|\mathcal{M}_{nk}^O|^2}{(\mathcal{M}_{nn}^D - \mathcal{M}_{kk}^D)^2} \delta_{mn}. \quad (85)$$

Then, we have

$$\begin{aligned} V_{51}^{(2)} &= \frac{1}{M_1} \sum_{k \neq 5} \frac{\mathcal{M}_{1k}^O \mathcal{M}_{5k}^O}{\mathcal{M}_{kk}^D} \\ &= \frac{1}{M_1} \left[\frac{g_1 \lambda (v_u^2 - v_d^2)}{2\sqrt{2}\mu_{\text{eff}}} + \frac{g_1 \lambda (v_u^2 - v_d^2)}{2\sqrt{2}\mu_{\text{eff}}} \right] = -\frac{g_1 \lambda v^2 \cos 2\beta}{\sqrt{2}M_1\mu_{\text{eff}}}, \end{aligned} \quad (86)$$

$$\begin{aligned} V_{52}^{(2)} &= \frac{1}{M_2} \sum_{k \neq 5} \frac{\mathcal{M}_{2k}^O \mathcal{M}_{5k}^O}{\mathcal{M}_{kk}^D} \\ &= \frac{1}{M_2} \left[-\frac{g_2 \lambda (v_u^2 - v_d^2)}{2\sqrt{2}\mu_{\text{eff}}} - \frac{g_2 \lambda (v_u^2 - v_d^2)}{2\sqrt{2}\mu_{\text{eff}}} \right] = \frac{g_2 \lambda v^2 \cos 2\beta}{\sqrt{2}M_2\mu_{\text{eff}}}, \end{aligned} \quad (87)$$

$$V_{53}^{(2)} = \frac{1}{\mu_{\text{eff}}} \sum_{k \neq 5} \frac{\mathcal{M}_{3k}^O \mathcal{M}_{5k}^O}{\mathcal{M}_{kk}^D} = 0, \quad (88)$$

$$V_{54}^{(2)} = -\frac{1}{\mu_{\text{eff}}} \sum_{k \neq 5} \frac{\mathcal{M}_{4k}^O \mathcal{M}_{5k}^O}{\mathcal{M}_{kk}^D} = 0. \quad (89)$$

Keeping all these terms, we can write

$$N_{51}^{(1)} + N_{51}^{(2)} = V_{51}^{(1)} + V_{51}^{(2)} = -\frac{g_1 \lambda v^2 \cos 2\beta}{\sqrt{2}M_1\mu_{\text{eff}}}, \quad (90)$$

$$N_{52}^{(1)} + N_{52}^{(2)} = V_{52}^{(1)} + V_{52}^{(2)} = \frac{g_2 \lambda v^2 \cos 2\beta}{\sqrt{2}M_2\mu_{\text{eff}}}, \quad (91)$$

$$N_{53}^{(1)} + N_{53}^{(2)} = \frac{1}{\sqrt{2}}(V_{53}^{(1)} + V_{54}^{(1)}) + \frac{1}{\sqrt{2}}(V_{53}^{(2)} + V_{54}^{(2)}) = -\frac{\lambda v \cos \beta}{\mu_{\text{eff}}}, \quad (92)$$

$$N_{54}^{(1)} + N_{54}^{(2)} = \frac{1}{\sqrt{2}}(-V_{53}^{(1)} + V_{54}^{(1)}) + \frac{1}{\sqrt{2}}(-V_{53}^{(2)} + V_{54}^{(2)}) = -\frac{\lambda v \sin \beta}{\mu_{\text{eff}}}. \quad (93)$$

For large $\tan \beta$, or more precisely, for $\lambda v \tan \beta / \mu_{\text{eff}} > 1$, N_{13} is very suppressed up to the second order. Thus, we include the third or higher order. The third order relation is given as

$$V_{nm}^{(3)} = - \sum_{p,q \neq n} \frac{\mathcal{M}_{mp}^O \mathcal{M}_{pq}^O \mathcal{M}_{qn}^O}{(\mathcal{M}_{mm}^D - \mathcal{M}_{nn}^D)(\mathcal{M}_{nn}^D - \mathcal{M}_{pp}^D)(\mathcal{M}_{nn}^D - \mathcal{M}_{qq}^D)} \quad (94)$$

$$- \sum_{p \neq n} \frac{3}{2} \frac{\mathcal{M}_{mn}^O |\mathcal{M}_{np}^O|^2}{(\mathcal{M}_{nn}^D - \mathcal{M}_{mm}^D)^2 (\mathcal{M}_{nn}^D - \mathcal{M}_{pp}^D)} \quad (95)$$

$$- \sum_{p,q \neq n} \frac{\mathcal{M}_{np}^O \mathcal{M}_{pq}^O \mathcal{M}_{qn}^O}{(\mathcal{M}_{nn}^D - \mathcal{M}_{pp}^D)^2 (\mathcal{M}_{nn}^D - \mathcal{M}_{qq}^D)} \delta_{nm}. \quad (96)$$

We here show only $V_{53}^{(3)}$ and $V_{54}^{(3)}$ since the other third order terms are negligible. In the third order, we have

$$V_{53}^{(3)} = -\frac{\lambda v^3}{2\sqrt{2}\mu_{\text{eff}}^2} \left(\frac{g_1^2}{M_1} + \frac{g_2^2}{M_2} \right) \cos 2\beta (\sin \beta + \cos \beta) + \frac{3\lambda^3 v^3}{2\sqrt{2}\mu_{\text{eff}}^3} \sin 2\beta (\sin \beta - \cos \beta), \quad (97)$$

$$V_{54}^{(3)} = -\frac{\lambda v^3}{2\sqrt{2}\mu_{\text{eff}}^2} \left(\frac{g_1^2}{M_1} + \frac{g_2^2}{M_2} \right) \cos 2\beta (\sin \beta - \cos \beta) + \frac{3\lambda^3 v^3}{2\sqrt{2}\mu_{\text{eff}}^3} \sin 2\beta (\sin \beta + \cos \beta), \quad (98)$$

and

$$N_{53}^{(3)} = -\frac{\lambda v^3}{2\mu_{\text{eff}}^2} \left(\frac{g_1^2}{M_1} + \frac{g_2^2}{M_2} \right) \cos 2\beta \sin \beta + \frac{3\lambda^3 v^3}{\sqrt{2}\mu_{\text{eff}}^3} \sin 2\beta \sin \beta, \quad (99)$$

$$N_{54}^{(3)} = -\frac{\lambda v^3}{2\mu_{\text{eff}}^2} \left(\frac{g_1^2}{M_1} + \frac{g_2^2}{M_2} \right) \cos 2\beta \cos \beta + \frac{3\lambda^3 v^3}{\sqrt{2}\mu_{\text{eff}}^3} \sin 2\beta \cos \beta. \quad (100)$$

Up to now, we have not sorted the eigenstates by magnitudes of eigenvalues. In the PQ-NMSSM, the singlino-like state is the lightest one in most parameter space. Therefore, we should change the mixing matrix in order to fit with the SUSY Les Houches Accord 2 convention [40], i.e. $N_{5i} \rightarrow N_{1i}$.

B Higgs-bottom quark and Higgs-gauge boson couplings

The CP-even Higgs mass matrix (33) can be diagonalized by the mixing matrix S according to the SLHA2 convention.

$$H_i^{\text{mass}} = S_{ij} H_j^{\text{weak}}, \quad (101)$$

where $H_i^{\text{weak}} = (H_{dR}, H_{uR}, S_R)$ and H_i^{mass} are ordered in increasing mass. Then the various Higgs couplings can be expressed by the components of the mixing matrix.

$$H_i b_L b_R^c : \quad \frac{y_b}{\sqrt{2}} S_{i1}, \quad (102)$$

$$H_i Z_\mu Z_\nu : \quad g_{\mu\nu} \frac{v(g_1^2 + g_2^2)}{\sqrt{2}} (S_{i1} \cos \beta + S_{i2} \sin \beta), \quad (103)$$

$$H_i W_\mu^+ W_\nu^- : \quad g_{\mu\nu} \frac{v g_2^2}{\sqrt{2}} (S_{i1} \cos \beta + S_{i2} \sin \beta). \quad (104)$$

C Higgs-neutralino couplings

Referring to Appendix A in [3], the Higgs-neutralino couplings in the PQ-NMSSM are given by

$$H_a \tilde{\chi}_i^0 \tilde{\chi}_j^0 : \frac{\lambda}{\sqrt{2}} (S_{a1} \Pi_{ij}^{45} + S_{a2} \Pi_{ij}^{35} + S_{a3} \Pi_{ij}^{34}) + \frac{g_1}{2} (S_{a1} \Pi_{ij}^{13} - S_{a2} \Pi_{ij}^{14}) - \frac{g_2}{2} (S_{a1} \Pi_{ij}^{23} - S_{a2} \Pi_{ij}^{24}), \quad (105)$$

where

$$\Pi_{ij}^{ab} = N_{ia} N_{jb} + N_{ib} N_{ja}.$$

Each term can be explained in piecewise. The first term denotes a th Higgs coupling to i th and j th neutralinos through the H_{dR} component of the a th Higgs with the \tilde{H}_u^0 and \tilde{S} components of the neutralinos, i.e. $\lambda H_{dR} \tilde{H}_u^0 \tilde{S} / \sqrt{2}$. The second and third terms are from permutations of the first term, i.e. $\lambda H_{uR} \tilde{H}_d^0 \tilde{S} / \sqrt{2}$ and $\lambda S_R \tilde{H}_d^0 \tilde{H}_u^0 / \sqrt{2}$. The fourth and fifth terms are from the SUSY $U(1)_Y$ gauge couplings of H_d and H_u multiplets. Likewise, the last two terms are from the SUSY $SU(2)_L$ gauge interactions.

References

- [1] For a review, see, J. E. Kim and G. Carosi, Rev. Mod. Phys. **82**, 557 (2010) [arXiv:0807.3125 [hep-ph]].
- [2] J. E. Kim and H. P. Nilles, Phys. Lett. B **138**, 150 (1984); E. J. Chun, J. E. Kim and H. P. Nilles, Nucl. Phys. B **370**, 105 (1992).
- [3] For a review, see U. Ellwanger, C. Hugonie and A. M. Teixeira, Phys. Rept. **496**, 1 (2010) [arXiv:0910.1785 [hep-ph]].
- [4] K. S. Jeong, Y. Shoji and M. Yamaguchi, JHEP **1204**, 022 (2012) [arXiv:1112.1014 [hep-ph]]; K. S. Jeong, Y. Shoji and M. Yamaguchi, arXiv:1205.2486 [hep-ph].
- [5] J. E. Kim, H. P. Nilles and M. S. Seo, arXiv:1201.6547 [hep-ph].
- [6] G. Aad *et al.* [ATLAS Collaboration], Phys. Lett. B **710**, 49 (2012) [arXiv:1202.1408 [hep-ex]]; S. Chatrchyan *et al.* [CMS Collaboration], Phys. Lett. B **710**, 26 (2012) [arXiv:1202.1488 [hep-ex]].
- [7] G. Aad *et al.* [The ATLAS Collaboration], arXiv:1207.7214 [hep-ex]; S. Chatrchyan *et al.* [The CMS Collaboration], arXiv:1207.7235 [hep-ex].
- [8] E. Aprile *et al.* [XENON100 Collaboration], arXiv:1207.5988 [astro-ph.CO].

- [9] C. Panagiotakopoulos and A. Pilaftsis, Phys. Rev. D **63**, 055003 (2001) [hep-ph/0008268]; A. Dedes, C. Hugonie, S. Moretti and K. Tamvakis, Phys. Rev. D **63**, 055009 (2001) [hep-ph/0009125].
- [10] A. Delgado, C. Kolda, J. P. Olson and A. de la Puente, Phys. Rev. Lett. **105**, 091802 (2010) [arXiv:1005.1282 [hep-ph]]; A. Delgado, C. Kolda and A. de la Puente, Phys. Lett. B **710**, 460 (2012) [arXiv:1111.4008 [hep-ph]].
- [11] J. C. Romao, Phys. Lett. B **173**, 309 (1986).
- [12] Y. Kanehata, T. Kobayashi, Y. Konishi, O. Seto and T. Shimomura, Prog. Theor. Phys. **126**, 1051 (2011) [arXiv:1103.5109 [hep-ph]]; T. Kobayashi, T. Shimomura and T. Takahashi, arXiv:1203.4328 [hep-ph].
- [13] M. Muhlleitner, A. Djouadi and Y. Mambrini, Comput. Phys. Commun. **168**, 46 (2005) [hep-ph/0311167]; U. Ellwanger, J. F. Gunion and C. Hugonie, JHEP **0502**, 066 (2005) [hep-ph/0406215]; U. Ellwanger and C. Hugonie, Comput. Phys. Commun. **175**, 290 (2006) [hep-ph/0508022]; G. Belanger, F. Boudjema, C. Hugonie, A. Pukhov and A. Semenov, JCAP **0509**, 001 (2005) [hep-ph/0505142]; U. Ellwanger and C. Hugonie, Comput. Phys. Commun. **177**, 399 (2007) [hep-ph/0612134]; D. Das, U. Ellwanger and A. M. Teixeira, Comput. Phys. Commun. **183**, 774 (2012) [arXiv:1106.5633 [hep-ph]].
- [14] S. Chatrchyan *et al.* [CMS Collaboration], arXiv:1207.1898 [hep-ex]; G. Aad *et al.* [ATLAS Collaboration], arXiv:1208.0949 [hep-ex].
- [15] K. Choi, K. S. Jeong and K. -i. Okumura, JHEP **0509**, 039 (2005) [hep-ph/0504037]; K. Choi, K. S. Jeong, T. Kobayashi and K. -i. Okumura, Phys. Rev. D **75**, 095012 (2007) [hep-ph/0612258]; K. Choi and H. P. Nilles, JHEP **0704**, 006 (2007) [hep-ph/0702146].
- [16] K. Nakamura *et al.* [Particle Data Group Collaboration], J. Phys. G **37**, 075021 (2010).
- [17] G. Abbiendi *et al.* [OPAL Collaboration], Eur. Phys. J. C **35**, 1 (2004) [hep-ex/0401026].
- [18] G. Aad *et al.* [ATLAS Collaboration], JHEP **1206**, 039 (2012) [arXiv:1204.2760 [hep-ex]].
- [19] A. Menon, D. E. Morrissey and C. E. M. Wagner, Phys. Rev. D **70**, 035005 (2004) [hep-ph/0404184]; V. Barger, P. Langacker and H. -S. Lee, Phys. Lett. B **630**, 85 (2005) [hep-ph/0508027]; V. Barger, P. Langacker, I. Lewis, M. McCaskey, G. Shaughnessy and B. Yencho, Phys. Rev. D **75**, 115002 (2007) [hep-ph/0702036]; C. Balazs, M. S. Carena, A. Freitas and C. E. M. Wagner, JHEP **0706**, 066 (2007)

- [arXiv:0705.0431 [hep-ph]]; J. Cao, H. E. Logan and J. M. Yang, Phys. Rev. D **79**, 091701 (2009) [arXiv:0901.1437 [hep-ph]]; W. Wang, arXiv:1205.5081 [hep-ph].
- [20] M. A. Shifman, A. I. Vainshtein and V. I. Zakharov, Phys. Lett. B **78**, 443 (1978); A. I. Vainshtein, V. I. Zakharov and M. A. Shifman, Sov. Phys. Usp. **23** (1980) 429 [Usp. Fiz. Nauk **131** (1980) 537].
- [21] J. R. Ellis, A. Ferstl and K. A. Olive, Phys. Lett. B **481**, 304 (2000) [hep-ph/0001005].
- [22] K. Choi, E. J. Chun and J. E. Kim, Phys. Lett. B **403**, 209 (1997) [hep-ph/9608222].
- [23] V. Khachatryan *et al.* [CMS Collaboration], Phys. Lett. B **698**, 196 (2011) [arXiv:1101.1628 [hep-ex]]; G. Aad *et al.* [ATLAS Collaboration], Phys. Lett. B **701**, 186 (2011) [arXiv:1102.5290 [hep-ex]]; G. Aad *et al.* [ATLAS Collaboration], Phys. Lett. B **701**, 398 (2011) [arXiv:1103.4344 [hep-ex]]; S. Chatrchyan *et al.* [CMS Collaboration], JHEP **1107**, 113 (2011) [arXiv:1106.3272 [hep-ex]]; S. Chatrchyan *et al.* [CMS Collaboration], JHEP **1108**, 155 (2011) [arXiv:1106.4503 [hep-ex]]; S. Chatrchyan *et al.* [CMS Collaboration], Phys. Rev. Lett. **107**, 221804 (2011) [arXiv:1109.2352 [hep-ex]]; G. Aad *et al.* [ATLAS Collaboration], Phys. Lett. B **710**, 67 (2012) [arXiv:1109.6572 [hep-ex]];
- [24] D. Das, U. Ellwanger and A. M. Teixeira, JHEP **1204**, 067 (2012) [arXiv:1202.5244 [hep-ph]].
- [25] D. A. Vasquez, G. Belanger, C. Boehm, J. Da Silva, P. Richardson and C. Wymant, arXiv:1203.3446 [hep-ph].
- [26] M. Lisanti, P. Schuster, M. Strassler and N. Toro, arXiv:1107.5055 [hep-ph].
- [27] G. Aad *et al.* [ATLAS Collaboration], JHEP **1111**, 099 (2011) [arXiv:1110.2299 [hep-ex]].
- [28] G. Aad *et al.* [ATLAS Collaboration], arXiv:1206.1760 [hep-ex].
- [29] G. Aad *et al.* [ATLAS Collaboration], arXiv:1207.4686 [hep-ex].
- [30] G. Aad *et al.* [ATLAS Collaboration], Phys. Rev. Lett. **108**, 181802 (2012) [arXiv:1112.3832 [hep-ex]].
- [31] G. Aad *et al.* [ATLAS Collaboration], arXiv:1208.1447 [hep-ex].
- [32] M. Bahr *et al.*, Eur. Phys. J. C **58**, 639 (2008) [arXiv:0803.0883 [hep-ph]]; S. Gieseke *et al.*, arXiv:1102.1672 [hep-ph].
- [33] J. Pumplin, D. R. Stump, J. Huston, H. L. Lai, P. M. Nadolsky and W. K. Tung, JHEP **0207**, 012 (2002) [hep-ph/0201195].

- [34] S. Oryn, X. Roubly and V. Lemaitre, arXiv:0903.2225 [hep-ph].
- [35] M. Cacciari, G. P. Salam and G. Soyez, JHEP **0804**, 063 (2008) [arXiv:0802.1189 [hep-ph]].
- [36] M. L. Mangano, M. Moretti, F. Piccinini, R. Pittau and A. D. Polosa, JHEP **0307**, 001 (2003) [hep-ph/0206293].
- [37] G. Aad *et al.* [ATLAS Collaboration], arXiv:0901.0512 [hep-ex].
- [38] D. R. Tovey, Eur. Phys. J. direct C **4**, N4 (2002).
- [39] K. J. Bae, R. Dermisek, H. D. Kim and I. -W. Kim, JCAP **0708**, 014 (2007) [hep-ph/0702041].
- [40] B. C. Allanach *et al.*, Comput. Phys. Commun. **180**, 8 (2009) [arXiv:0801.0045 [hep-ph]].